2019

Manifoldlike Causal Sets

Miremad Aghili
University of Mississippi

Manifoldlike Causal Sets

A Dissertation
presented in partial fulfillment of requirements
for the degree of Doctor of Philosophy
in the Department of Physics and Astronomy
The University of Mississippi

by

Miremad Aghili

May 2019

ABSTRACT

The content of this dissertation is written in a way to answer the important question of manifoldlikeness of causal sets. This problem has importance in the sense that in the continuum limit and in the case one finds a formalism for the sum over histories, the result requires to be embeddable in a manifold to be able to reproduce General Relativity. In what follows I will use the distribution of path length in a causal set to assign a measure for manifoldlikeness of causal sets to eliminate the dominance of nonmanifoldlike causal sets. The distribution of interval sizes is also investigated as a way to find the discrete version of scalar curvature in causal sets in order to present a dynamics of gravitational fields.

DEDICATION

Every journey comes to an end and I am very happy that my journey ended in the Department of Physics and Astronomy at the University of Mississippi. The invaluable lessons I learned and excellent people that I met in this journey has changed my life forever.

In the beginning, I would like to thank my committee, Dr. Beach, Dr. Stein, and Dr. Buskes for their useful comments which made it possible for me to do a better job.

Secondly, I want to thank my incredible supervisor, Dr. Bombelli, who, in addition to being a beautiful person, taught me how not to be judgmental of people and that is one lesson I will never forget. He taught me how to be an independent researcher, and with his insightful comments showed me there is always another angle to look at the problem. I would like to thank him for not laughing at my ideas and for his support which made my stay at Oxford better than a dream.

I would also like to thank my family for their love and their constant support of my passion for physics and their help. I thank them for sacrificing their youth to protect me. Because if it was not for their help I would not be here right now. I thank them for being wonderful role models.

Finally, I want to dedicate my dissertation to my lovely wife, who kept up with me all these years, through ups and downs and through bitter and sweet and always supported me and pushed me. She never gave up on me and stayed by my side, and that is the reason I was able to finish my Ph.D., far from home and family. I dedicate this small present to many nights that she did not sleep, thinking about our future.

Many thanks to many of my friends especially Mrs. Mahdi, Dr. Shariat-madar, Mr. & Mrs. McKenzie and Mr. & Mrs. Reeder, who helped us through these years and made our life wonderful.

ACKNOWLEDGEMENTS

I would like to thank the department of Physics and Astronomy at the University of Mississippi for supporting me during my studies and also Graduate School for partially supporting my research.

TABLE OF CONTENTS

LIST OF FIGURES

CHAPTER 1

INTRODUCTION

The main topic of this dissertation is an approach to quantum gravity. If coupled to matter fields quantum gravity can be considered as a "theory of everything," able to remove the current shortcomings of existing theories. This program is started with the hope that it can unify matter fields and their interactions. Regarding that matter, I give a very brief explanation.

The theory of general relativity is extremely precise at large scales (larger than Planck scale) and so far its predictions have been verified by accurate measurements and observations, such as the recent detection of gravitational waves, which has changed the perspective in physics and introduced us to a whole new observation method, known as multi-messenger astronomy. However, the small-scale/high-energy situations are a challenge for the theory. The predictions by general relativity in those regimes include singularities, such as the ones that exist inside black holes and the big bang. In addition, the theory as it is, is not renormalizable by the common methods.

At the other end in the nuclear and sub-nuclear regime, Quantum Field Theory (QFT) and in particular the Standard Model has had a huge success in unifying Electromagnetism and Weak forces and a indication of possible unification with Strong force and predictions of many scattering amplitudes and physical phenomena with high precision. However, it is also unable to describe some phenomena such as the matter-antimatter asymmetry, dark matter, ultraviolet divergences etc. Currently many groups are working on physics beyond the standard model where some of these theories has inspired some approaches to quantum gravity such as lattice quantum gravity [1].

A new theory that is able to combine gravity and QFT in the correct way might be able to resolve the above issues and also help achieve a consistent theory of gravity coupled to matter fields, which are treated as quantum.

1.1 Alternative Theories of Gravity

Alternative theories of gravity usually consist of some modification of the Einstein formulation of gravity, to overcome some of the difficulties posed by the singularities such as the ones predicted inside black holes. Some of the theories, such as Scalar-Tensor gravity, looking for new physics, couple extra fields with some parameters to gravity through action in order to investigate the predictions and outcome of the observation of black holes, neutron stars, cosmology, gravitational waves etc, assuming these fields exist. An example of such theories is Brans-Dicke theory [2].

Another class of popular alternative theories of gravity are the ones that include higher order curvature terms in the Lagrangian of the theory. The initial motivation for these theories was to resolve the renormalizability of the theory. However, the number of terms that needs to be included is not finite which is a reason for people to pursue other approaches.

Some other theories make more dramatic changes to the nature of gravity such as Bimetric Gravity [3] in which the theory of gravity is explained by introducing two metrics. If one of the two metrics is used at higher energy scales, it can enable theories in which speed of light can vary. Bimetric theory of gravity can also be used for modeling massive gravitons.

These theories are able to make some predictions about large scale phenomena that are interesting to observe. Using a wide range of observations from gravitational waves and black holes to the expansion of the universe, for observation of the types of the waves, the shape of the waves or the radiation, one can test these predictions. The parameters that these theories introduce can be tuned or bounded by these observations and some of them

might even be disqualified (for a good review, see Ref. [4]).

1.2 Quantum Gravity

There are many reasons for a physicist to think that at the very small scales and high energies the theory governing the universe should be fundamentally different from general relativity, among which one reason are the singularities that the theory of general relativity can not avoid such as black holes and the big bang and nonrenormalizability.

A different approach to the problem is used by various theories of quantum gravity, including String Theory, Causal Dynamical Triangulations (CDT), Noncommutative Geometries, Loop Quantum Gravity (LQG), and Causal Set Theory (CST). We will talk extensively about the latter in the next section.

The common factor between all of these theories is that except for string theory they all deal with geometry as the basic quantity describing spacetime and gravity, and try to change the treatment of geometry in a fundamental way in order to resolve the issues faced by the theory of General Relativity.

In many of the approaches the continuum geometry is replaced by a discrete structure, either as a consequence of the theory or as the starting point. The discreteness of the geometry has an immediate benefit as there is no longer a manifold structure at arbitrarily small scales, which is the main reason for infinite curvature predicted inside black holes and in cosmology.

In the case of Quantum Gravity, unlike alternative theories of gravity, it is much harder to come up with large scale phenomenology, because the strongest quantum effects happen at Planck scale, and therefore a direct measurement is not possible and many indirect measurements of quantum effects might not be observable at large scales.

At the scales of order Planck scale, no experiments can be performed because any type of measurements that would be able to detect such small sizes require probes with a very short wavelength which carry a lot of energy and would change the background structures

drastically, making it impossible to observe any effects.

Here I will only mention the general picture of how some of these approaches work.

Noncommutative Geometry

Many properties of a geometric space X can be obtained by the set of smooth functions from the space X to $\mathbb{R}$ and their algebra. In the case of a regular manifold this algebra is commutative, however one can generalize this concept to include algebra whose elements do not commute, and therefore define a noncommutative generalizations of the manifold. These generalized types are called noncommutative geometries. A way to create a noncommutative geometry is to force the coordinates not to commute

$$[x^\mu, x^\nu] = i\theta^{\mu\nu}. \tag{1.1}$$

This type of algebra is not new in physics. In quantum mechanics and quantum field theory noncommutative algebras are present, and in particular they are responsible for the Heisenberg uncertainty principle. Since this approach works well for QFT then it motivates some of the scientists to apply it to gravity.

Noncommutative geometry couples gravity to the matter fields using the same type of algebras [5], and therefore for a theory for quantum gravity it is logical to assume that the uncertainty of the coordinates $\sqrt{\theta} \approx \ell_{\mathrm{P}}$, and ℓ_{P} is the Planck length. The existence of the uncertainty in the location at the smaller scales is what gives the scientists in these areas hope to avoid singularities.

String Theory

The Bosonic String Theory initially started as a candidate for the description of the strong force in the 1960s and later it was abandoned for the Quantum Chromodynamics (QCD). The reason that Bosonic String Theory did not work for the strong interactions was that it required a massless particles of spin 2 which there was no evidence for to exist in

strong interactions.

The same reasons, which make String Theory not promising for the description of strong interactions, make it a promising candidate for quantum gravity. Bosonic String Theory later was generalized to Superstring Theory to describe the unified approach including Fermions. In String Theory the particles can be interpreted as different modes of one-dimensional objects called strings, and one of these fundamental modes represents the graviton, the particle that has spin 2 and is conjectured to be the mediator for the gravitational field.

For a while different versions of the theory which where all consistent were being developed until in the 1990s it was conjectured that they are all limiting cases of a single theory in 11 dimensions named M-theory.

One of the major achievements of this theory is Anti de Sitter/Conformal Field Theory (AdS/CFT) correspondence which provides a nonperturbative formulation of string theory with some boundary conditions. In 1997 string theorists found out that on the boundary of the AdS spacetime which is a vacuum solution to the Einstein's equation with a negative cosmological constant, the string theory is equivalent to the quantum field theory and its results can be used as nonperturbative solutions to quantum field theory.

The large number of dimensions in the theory whose existence we have no evidence for yet, is one of the points that this theory is being criticized for. The solution that the string theorists propose for this problem is compactifying the dimensions which means that they assume that those extra dimensions fold on themselves. However, there is a non-uniqueness in the way compactification is carried out which is not ideal.

Loop Quantum Gravity

In this approach one uses the canonical formalism to create the Hamiltonian for the gravitational field. Since the Hamiltonian is the time evolution operator, using the canonical formalism to quantize the gravitational field with the same procedure that is used for matter

fields and their interactions seems to be equivalent to abandoning the covariance and choosing a special frame, although due to the freedom of choice of lapse and shift,[1] in this approach, the measured physical quantities will not change by choice of a different frame and therefore the case is not very severe.

In previous canonical formulations the algebra used was the one generated by the spatial metric and its conjugate momentum, but Ashtekar showed [7] that if one uses suitable connections and triads of spatial vectors as the actual variables, the algebra becomes much simpler. In this theory the volume and area operators turns out to have quantized eigenvalues which effectively makes space discrete.

Loop Quantum Cosmology (LQC) is a branch of LQG that is simplified in the sense that it has fewer degrees of freedom that LQG itself, and it has been applied to cosmology. Therefore it can be considered as a phenomenological aspect of LQG. From the most notable achievements of LQC one can mention the big bounce that replaces the big bang. According to LQC, the universe that existed before has gone under a collapse and then at some small scale, approximately Planck scale, has had a bounce and inflated again.

Causal Dynamical Triangulations

In this approach the choice of the coordinate is more severe than in LQG, as for the quantization of the geometry in CDT one needs to slice the spacetime into spacelike hypersurfaces and tile them with $(d-1)$-dimensional simplices of unit side length (in Planck units), and different time slices are also separated by a unit Planck length. The d-dimensional simplices are in contact with each other through $(d-1)$- dimensional surfaces. This type of discretization is a modification of Regge calculus, where the length of the sides of the simplices as discussed are kept fixed and is a very well understood topic in mathematics. At the intersection of the simplices the space is flat, but in a larger scale the way that the simplices are put together can impose some curvature on the spacetime.

[1]Lapse function and shift vector are the components of the metric whose change corresponds to the change of spacetime foliation.

There are many interesting results that are obtained from this approach. The studies have shown, that the dimension obtained from the diffusion process shows a decreasing pattern known as dimensional reduction at the smaller scales, and converges to 1.5, which is in agreement with the asymptotic safety scenario[6]. The dimension in the diffusion process estimated by using the timescale that it takes for a random walker to start from a point and come back to the same location. The physicists in favor of asymptotic safety scenario claim that the finite-temperature field theory, where temperature sets a scale on all dimensionful quantities, using dimensional analysis one can find

$$S = a(RT)^{d-1},\ E = bR^{d-1}T^d, \tag{1.2}$$

where S and E are the entropy and energy of the renormalizable gravitational field respectively, R is the scalar curvature, T is the temperature and a and b are some dimensionless constants. Rearranging the above formula to find the relationship between the Entropy and Energy

$$S \sim E^{\frac{d-1}{d}}. \tag{1.3}$$

On the other hand, one expects the high energy spectrum of a spacetime in general relativity to be dominated by black holes. In a spacetime with a nonzero cosmological constant such as Anti de Sitter, the entropy of a black hole scales as

$$S = \frac{A}{4G_N} \sim \left(\frac{MR_{\mathrm{AdS}}}{\ell_{\mathrm{P}}}\right)^{\frac{d-2}{d-1}}, \tag{1.4}$$

where A is the volume of the horizon. Therefore

$$S \sim E^{\frac{d-2}{d-3}}, \tag{1.5}$$

which is the same as the prediction of conformal theory with one lower dimension. For the de

Sitter case, which is more relevant for our universe, the results are not very well understood. According to Eqs. (1.3) and (1.5), it is obvious that these two predictions do not agree unless the dimension is 1.5.

Finally, due to the already time sliced nature of spacetime in this method it is also easier to write down the action evolve the spacetime between two identified initial and final spatial states, and finds its possible large-scale outcomes and predictions.

1.3 Causal Set Theory

Causal Set Theory (CST) was introduced in the 1980's by Sorkin, Bombelli, Lee, and Meyer [8] based on works by Myrheim [9], 't Hooft [10], Hawking [11] and Malament [12]. According to CST spacetime at Planck's scale is composed of discrete events (spacetime "atoms") that are related by a partial order relation $\prec$, interpreted as causality. This assumption reduces the spacetime to a locally finite partially ordered set.[2] Locally finite means that the cardinality of any interval $I(x, y) := \{z | x \prec z \prec y\}$ is finite. In general a partial order[3] is a relation satisfying the following properties

- Irreflexive:[4] $x \not\prec x \; \forall x$
- Transitive: $x \prec y \;\&\; y \prec z \Rightarrow x \prec z \; \forall x, y, z$.

The information on which pairs $x \prec y$ are related in a causal set can be represented by two types of matrices of 0s and 1s with the same amount of information, the *Relations* matrix $\mathbf{R}$ and the *Link* matrix $\mathbf{L}$. In the *Relations* matrix the ones represent the timelike related pairs,

$$R_{ij} = \begin{cases} 1 \; x_i \prec x_j \\ \\ 0 \text{ otherwise} \end{cases} , \tag{1.6}$$

[2] This way of thinking is also true for the continuum but the size of each interval is uncountably infinite.
[3] A partial order with the local finiteness condition is called a *causal set* or *causet* in the literature
[4] Many different papers use the reflexive convention for causal sets in which this condition is replaced by $\forall x, x \prec x$. While both conventions are correct and equivalent, we use the irreflexive convention. Note that if we use the reflexive definition we need an additional antisymmetry condition $x \prec y \;\&\; y \prec x \Rightarrow x = y$, in order to avoid closed timelike loops.

and in the *Link* matrix the ones represent the nearest timelike neighbors,

$$L_{ij} = \begin{cases} 1 \ x_i \prec\!\!* \, x_j \\ \\ 0 \text{ otherwise} \end{cases} , \tag{1.7}$$

here we use the notation $x \prec\!\!* \, y$ to indicate that x and y are nearest neighbors and therefore the interval $I(x, y)$ is empty. It can be seen that the Relations matrix can be obtained from the Link matrix by applying the transitive rules. Notice that the entries in the $\mathbf{R}$ and $\mathbf{L}$ matrices are always mostly 0s, since $R_{ii} = L_{ii} = 0$ for all i, and $(R_{ij} = 1) \Rightarrow (R_{ji} = 0)$ for all (i, j), with L_{ij} satisfying an analogous property; also, for each poset of this type there exists an integer $l \leq N + 1$ such that $\mathbf{R}^l = \mathbf{L}^l \neq \mathbf{0}$ but $\mathbf{R}^{l+1} = \mathbf{L}^{l+1} = \mathbf{0}$ as matrices.

The knowledge of the light cone structure and the volume element at every point in a sufficiently causal spacetime was shown by Hawking and Malament to be enough to determine the manifold structure and the metric up to a conformal factor. Later on it was shown by Bombelli and Meyer [13] that the same results can be extended to the dense subsets of manifolds, and finally in the causal set program it is conjectured that the *Relation/Link* matrix and the number of points enclosed in an interval (representative of the volume in CST) suffice for approximating the continuum spacetime, if the spacetime is past and future distinguishing.[5]

Before we move on with the rest of the introduction it is useful to define some of the terminology that will be used in this dissertation. An Alexandrov neighborhood of is defined as $\mathcal{A}(x, y) = I^+(x) \cap I^-(y)$, where $I^\pm$ is the chronological future/past of points $x \prec y$. An interval corresponds to the discrete version of Alexandrov neighborhoods, where it will be defined as $I(p, q) = \{s | p \prec s \prec q\}$. A chain of length k is defined as a sequence of k points that are causally related to each other, $chain : p_1 \prec p_2 \prec \cdots \prec p_k$, and paths are defined as the maximal chains in the sense that they could not be lengthened by adding another

[5] A past and future distinguishing manifold is one in which no two spacelike separated points have the same past or future.

point in the causal set to the sequence and therefore all the elements are nearest neighbors (linked) to each other, $path : p_1 \prec * p_2 \prec * \cdots \prec * p_k$.

1.3.1 Kinematics

In general, by Kinematics of causal sets we mean the study of the relationship between causal sets and continuum geometries. A basic question arises here and that is whether a causal set represents a manifold and if so, can the manifold that the causal set is approximating be determined uniquely, solely by looking at the causal relations. This leads us to the main conjecture of the theory

"**Hauptvermutung**": *If a causal set can be faithfully embedded in two different Lorentzian manifolds, then the manifolds must be close down to scales determined by the density.*

Progress towards a proof of this conjecture for the case of distinguishing manifolds has been made, and results can be found in an unpublished paper by Bombelli et al. in Ref. [14, 15].

In general, the kinematics of CST includes estimation of the manifoldlikeness, dimension, timelike and spacelike distances, curvature, as well as the effect of nonlocality, as will be discussed below.

It is known that in the macroscopic limit the universe and matter fields tends to be very well described by theories living on a continuous manifold, and obey general relativity/QFT with a great accuracy. A causal set is called manifoldlike if its elements can be embedded faithfully in a manifold. A faithful embedding is a map that embeds the causal set points in the manifold with uniform density, preserves the causal relations, and the manifold that it represents does not have any structure on scales smaller than the characteristic length defined by the density of the distribution. Obtaining a manifoldlike causal set at random is extremely unlikely. In fact as follows from the results in Ref. [16], as the number of points increases the probability that a generic causal set approximates a continuum manifold rapidly decreases. In the large-N limit the ratio of number of causal sets that are known as Kleitman-Rothschild (KR) orders to the total number of causal sets that can be generated approaches one.

A KR order is a three-level causal set in which half of the points are in the second level and the first and third level each have a quarter of the points, such that on average each point from the first and third level are connected to half of the points in the middle layer. Such a partial order is very unlikely to be embeddable in a manifold and if it is, it will not be embedded uniformly in any dimensions. The reason is that they are very short, and therefore in order to be able to embed them in the manifold, the manifold requires a high number of dimensions and the height scale of the manifold would be of the order of the average distance between points which is in contrast to the "no structure at small scales" assumptions of faithful embedding, and there will not be enough points to get good statistics of the structure of the spacetime.

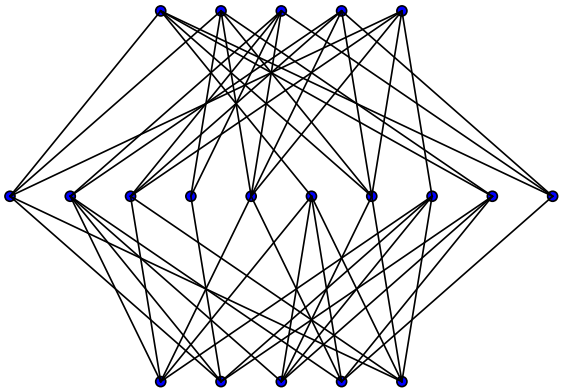

The domination of the KR causal sets causes two major problems. First, this very huge suppression of anything manifoldlike and should be addressed somehow in an action for the theory. Second, there not yet exists a way to randomly generate causal sets that are uniformly distributed in the space of causal sets, However, even if there was, due to the KR effect it will take a long amount of time to get enough samples of any type of manifoldlike or nonmanifoldlike causal set that are not of the KR type.

One way to obtain some manifoldlike causal sets to work with is to sprinkle points at random uniformly in an already existing manifold and deduce the relations from the metric. The randomness is necessary for preserving the Lorentz invariance at least in the case of

flat spacetime where there exists no preferred frame[18]. There is no proof that this is the only way that the points can be sprinkled in a general spacetime manifold in order to have a generally covariant procedure, however, for the case of Minkowski this looks like to be the only choice, because the spacetime itself is symmetric in every direction.

In CST the Lorentzian symmetry is considered more fundamental than the concept of locality, which can be understood by looking at the manner that the discretization is done. The concept of locality is abandoned in CST due to the nature of causal relations. Since in any given frame, a point that is arbitrarily far away in a spatial sense can be nearest neighbor to another point as long as they are near each other's light cone, therefore, being linked to another element in a causal set does not necessarily mean that they are spatially close. Therefore, the new infinities (such as number the of nearest neighbors) introduced by CST by removing the continuum infinities needs to be addressed properly.

Locality:

With regards to measuring the spatial distances, a method is proposed for the case of two dimensions, however it can not be extended to higher dimensions. As suggested by this method, we take two spacelike-related points x and y and we find their common past and common future. Then in each of these sets we choose a point, z_{past} and z_{future} respectively, such that they minimize the spacetime distance $L_{\text{past}} = L(z_{\text{past}}, x) + L(z_{\text{past}}, y)$ and $L_{\text{future}} = L_(x, z_{\text{future}}) + L_(y, z_{\text{future}})$ respectively. Once z_{past} and z_{future} are recognized we can approximately assume that the spatial distance between x and y is equal to the height of the intersection of the chronological past of z_{future} and the chronological future of z_{past}. For higher dimensions, especially for 4 and more, this method does not converge to the correct value due to the high number of minimizing points [19].

In past years there have been some nice efforts to identify local regions in causal sets, Ref. [20]. In the mentioned paper, the authors use the distribution of Alexandrov neighborhoods contained in a larger Alexandrov neighborhoods to define local neighborhoods.

For a fixed number of points N in a volume V_0 the probability of finding k points in a smaller volume V inside V_0 is obtained from the binomial distribution,

$$P_k = \binom{N}{k}\left(1-\frac{V}{V_0}\right)^k\left(\frac{V}{V_0}\right)^k,$$

which can be approximated by the Poisson distribution when the ratio V/V_0 tends to zero

$$P_k = \frac{(\rho V)^k}{k!}\mathrm{e}^{-\rho V},$$

where $\rho = N/V_0$ is the average density of the distribution. The authors show that by using the Poisson approximation in the causal set the volume distribution of smaller Alexandrov neighborhoods has the form

$$\begin{aligned}\langle a_k^{(d)}\rangle = &\frac{N^{k+2}}{(k+2)!}\frac{\Gamma(d)^2}{\left(\frac{d}{2}(k+1)+1\right)_{d-1}}\frac{1}{\left(\frac{d}{2}k+1\right)_{d-1}}\times \\ &{}_dF_d(\{1+k,\tfrac{2j}{d}+k\},\{3+k,\tfrac{2j}{d}+k+2\}|-N), j=1,\cdots,d-1 \end{aligned} \tag{1.8}$$

where $a_k^{(d)}$ is the average number of intervals of volume k, ${}_dF_d$ is a hypergeometric function of order d, and $(w)_n := \Gamma(w+1)/\Gamma(w-n+1)$, with w here an integer or half integer. The shape of the distribution remains reasonably unchanged in curved spacetimes such as de Sitter compared to the Minkowski distribution for Alexandrov neighborhoods with smaller sizes. Therefore they conjecture that a causal set $\mathcal{C}$ whose Alexandrov neighborhoods distribution approximately resembles the one in Eq. (1.8) for a fixed dimension d, i.e, $a_k^{(d)}(\mathcal{C}) \approx \langle a_k^{(d)}\rangle(N \pm \sqrt{N})$ for all k are local intervals in the same sense that one can approximate a local neighborhood by Minkowski metric in the continuum. The statistical considerations are obtained from the assertion that the distribution of causal set points in the manifold is that of Poisson distribution.

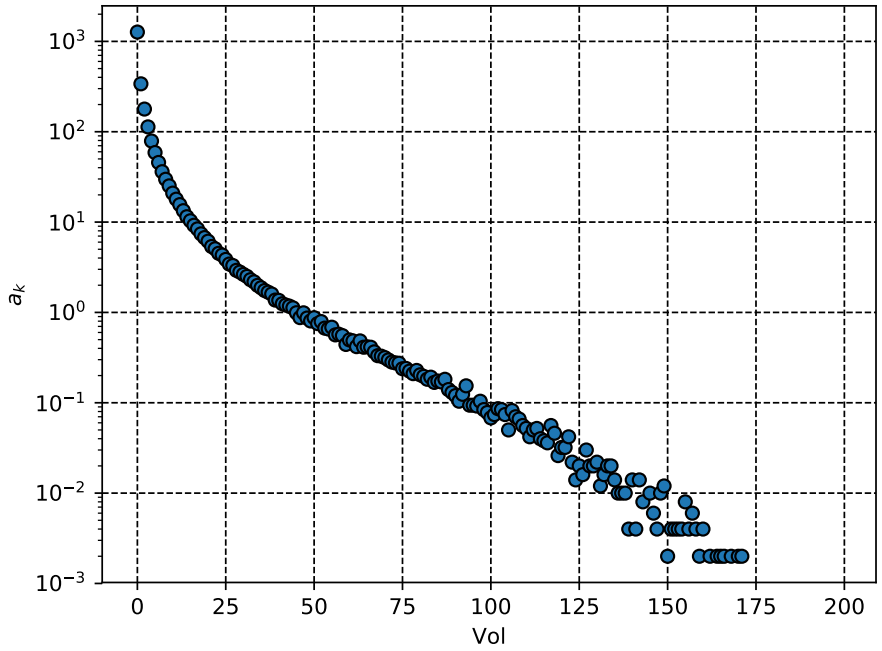

Figure 1.1. Abundance of Alexandrov neighborhoods of various sizes (volumes) with in an Alexandrov neighborhood of size 200 points, averaged over 200 sprinklings in a 4-dimensional Minkowski spacetime.

Dimension:

A number of definitions of dimension for posets are available. For the sake of a review for one of the later chapters we go into the details of some that are of interest to us. These are the definitions that when applied to large posets obtained from uniform sprinklings of points in d-dimensional Minkowski space give d as the result. The definition of dimension of a poset normally used in combinatorics [21] does not have this property, except when $d = 2$.[6] The available definitions that do have this property are all probabilistic in nature, and can be used to determine the effective dimensionality of different regions within a poset and at different scales, in general with varying results, and come in two kinds. In the first

[6]Mathematical definition of dimension of a partially ordered set P is the least number of chains whose product contains P as a subset.

kind [22, 23, 24, 25], local neighborhoods are identified with intervals $A(p,q)$ within which combinatorial properties of the poset are analyzed, and their volume (cardinality) is used as a measure of the size of each neighborhood. The second kind of definition, that of spectral dimension [26, 27, 28], uses a diffusing particle that executes a random walk starting from a given poset element and following links between elements to identify a local neighborhood around that point, and the scale is determined by the number of steps the particle is allowed to take.

Midpoint Approach

The midpoint dimension of a poset [22] is obtained as follows. Having two related points p, q in $\mathcal{C}$, choose a points p_m in $\mathcal{C}$ such that the cardinality, n, of the smaller of the two resultant intervals $A_\downarrow = A(p,p_m)$ and $A_\uparrow = A(p_m,q)$ is as large as possible. If the overall N is large enough, then this point is most likely in the middle of the big interval, in the sense that the two smaller intervals will have approximately equal volumes and they will be the largest ones for which this is the case. If $\mathcal{C}$ was uniformly embedded in a flat continuum spacetime, the height of each of $A_\downarrow$ and $A_\uparrow$ would then be approximately half of that of $\mathcal{C}$ and, because their volumes V scale as the d-th power of their height we would have approximately,

$$v = \frac{V}{2^d} \ , \tag{1.9}$$

where V is the volume of $A(p,q)$, and v the volume of the smaller of $A_\downarrow$ and $A_\uparrow$, in the continuum. But in a poset obtained from a Poisson sprinkling of points in a manifold, the number N of poset elements in each region is proportional to its volume, $N = \rho V$, where ρ is the sprinkling density. As a result, in this approach the Minkowski dimension of the set can estimated as

$$d = \frac{\ln(N/n)}{\ln(2)} = \log_2(N/n) \ . \tag{1.10}$$

Modified Myrheim-Meyer Approach

The Myrheim-Meyer method to estimate the dimension of a poset [23] relies on analytical results on the mean number of chains of length k, denoted by $\langle C_k \rangle$ in an N-element Minkowski poset. This number depends on the dimensionality d, and is given in Ref. [23] by

$$\langle C_k \rangle = N^k \left(\frac{\Gamma(d+1)}{2} \right)^{k-1} \frac{\Gamma(d/2+1)\,\Gamma(d)}{\Gamma(k\,d/2+1)\,\Gamma((k+1)d/2)} \,. \tag{1.11}$$

A slight modification to this result, that monotonically increase as k becomes larger, was introduced recently [39],

$$\langle C_k \rangle = \frac{N!}{(N-k)!} \left(\frac{\Gamma(d+1)}{2} \right)^{k-1} \frac{\Gamma(d/2+1)\,\Gamma(d)}{\Gamma(k\,d/2+1)\,\Gamma((k+1)d/2)} \,. \tag{1.12}$$

The proof of the above modification is provided elsewhere [39].

To use this result, we choose a specific value of k and solve for d the resulting relation. Choosing $k = 2$, for example, we can estimate the dimension of a flat space in which a poset is uniformly embedded by solving for d the equation

$$\frac{\langle C_2 \rangle}{N(N-1)} \approx \frac{1}{4} \frac{\Gamma(d+1)\,\Gamma(d/2)}{\Gamma(3d/2)} \,, \tag{1.13}$$

which can be done numerically using the abundance of chains of length 2, i.e., the number of related pairs of elements in the poset, for $\langle C_2 \rangle$.

Brightwell-Gregory Approach

The Brightwell-Gregory method [24] for calculating the dimension of a Minkowski poset is based on the length of the longest path in the poset. If an N-element poset is uniformly sprinkled inside an Alexandrov neighborhood of volume V in Minkowski space, the longest path (longest chain) in it can be thought of as a discretized geodesic between the maximal and minimal points. Its length $k_{\max}$ should then be approximately proportional to

the proper time from p_0 to p_{N+1}, which in the continuum is in turn proportional (with a known proportionality coefficient) to $V^{1/d}$. This leads to defining a coefficient $\beta_{d,N}$ by

$$k_{\max} = \beta_{d,N}\, N^{1/d} \,. \tag{1.14}$$

This $\beta_{d,N}$ is expected to be only weakly dependent on N and in the large-N limit, when endpoint effects become unimportant, it should approach a well-defined value

$$\beta_d := \lim_{N\to\infty} \beta_{d,N} \,. \tag{1.15}$$

Brightwell and Gregory found [24] that in two dimensions $\beta_2 = 2$, and for arbitrary dimensionality $d \geq 3$ we have

$$1.77 \leq \frac{2^{1-1/d}}{\Gamma(1+1/d)} \leq \beta_d \leq \frac{2^{1-1/d}\, \mathrm{e}\, \Gamma(d+1)^{1/d}}{d} \leq 2.62 \,. \tag{1.16}$$

These upper and lower bounds on β_d are plotted as functions of d in figure 4.6. We can both infer from such plots and find analytically that $\beta_d \to 2$ as $d \to \infty$, and these results are consistent with $\beta_d = 2$ for all d, but we are not aware of results to this effect. It is interesting to note that, while these bounds allow a greater range of values for β_d above 2 than below 2, it appears from the results of our simulations, shown in figure 4.7, that for low values of N all $\beta_{d,N}$ are below 2.

In this approach, the Minkowski dimension of a given poset can be estimated by finding $k_{\max}$ and solving for d the defining relation for $\beta_{d,N}$, that can be written as

$$d = \frac{\ln(N)}{\ln(k_{\max}/\beta_{d,N})} \,. \tag{1.17}$$

1.3.2 Dynamics

The dynamics of CST deals with defining a gravitational action for causal sets and an action for each type of matter field defined on the causal sets, for example a scalar field action, which is not an easy task given that it is a nonlocal theory. For each of the above problems there are some proposals. We start by discussing the gravitational action and then move on to the others.

One of the methods introduced to address the above problem is the Classical Sequential Growth [17], which unfortunately is unable to create realistic manifoldlike causal sets. This procedures requires adding the points to the causal set one by one based on some probability rules. The causal sets that are obtained this way are usually either too short and fat or very long and thin, unable to represent anything close to a physical spacetime.

Scalar Curvature:

Fay Dowker et al. in Ref. [29] found an expression for a discrete version of the d'Alembertian $B^{(d)}$, to find the causal set version of scalar curvature which in the continuum, this is equivalent to the gravitational Lagrangian

$$B^{(2)}\phi(x) = \frac{2}{l^2}(- \underbrace{\phi(x)}_{\substack{\text{local}\\ \text{contributions}}} + \underbrace{(\sum_{y\in L_1} -2\sum_{y\in L_2} +\frac{1}{2}\sum_{y\in L_3})\phi(y))}_{\text{nonlocal contributions}} \tag{1.18}$$

$$B^{(4)}\phi(x) = \frac{4}{\sqrt{6}l^2}(- \underbrace{\phi(x)}_{\substack{\text{local}\\ \text{contributions}}} + \underbrace{(\sum_{y\in L_1} -9\sum_{y\in L_2} +8\sum_{y\in L_3} -\frac{4}{3}\sum_{y\in L_4})\phi(y))}_{\text{nonlocal contributions}} \tag{1.19}$$

where $\phi(x)$ is the scalar field at location x, and L_i is the set of inclusive intervals of volume $(i-1)$, $L_i := \{y \in \mathcal{C} : y \prec x \text{ and } n(x,y) = i-1\}$. Numerical calculations show that this proposal suffers from huge fluctuations, and therefore they define a regulator that makes

these fluctuations die away like $N^{1/2}$ for large causal sets. In the $d = 4$ case this leads to

$$B_k\phi(x) = \frac{4}{\sqrt{6}l_k^2}\left[-\phi(x) + \epsilon\sum_{y\prec x} f\left(n(x,y),\epsilon\right)\phi(y)\right], \tag{1.20}$$

where $\epsilon = (l/l_k)^4$ and

$$f(n,\epsilon) = (1-\epsilon)^n\left[1 - \frac{9\epsilon n}{1-\epsilon} + \frac{8\epsilon^2 n!}{(n-2)!(1-\epsilon)^2} - \frac{4\epsilon^3 n!}{3(n-3)!(1-\epsilon)^3}\right], \tag{1.21}$$

$l \ll l_k \ll L$ is some intermediate scale, and L is the size of the scalar field support. The expectation value of B in (1.18), (1.19) with the damping reproduces the d'Alembertian in the continuum limit in Minkowski spacetime and in curved spacetimes by using Riemann Normal Coordinates (RNC) they find

$$\lim_{l_k\to 0}\left\langle B_k^{(i)}\phi(x)\right\rangle = \left(\Box + \frac{1}{2}R(x)\right)\phi(x) \tag{1.22}$$

Applying the proposed discrete d'Alembertian to a constant scalar field of value 2 and some compact support one finds a discretized version of the scalar curvature.

The action obtained from this proposal is useful for finding transition amplitudes, but not equations of motion. There is no proof that it is able to suppress nonmanifoldlike causal sets. An important point to be made is that the coefficients and the number of layers considered in the proposed action are dimension dependent, even for the simplest choice of number of layers one might use

$$\frac{1}{\hbar}S^{(2)}[\mathcal{C}] = N - 2N_1 + 4N_2 - 2N_3, \tag{1.23}$$

$$\frac{1}{\hbar}S^{(4)}[\mathcal{C}] = N - N_1 + 9N_2 - 16N_3 + 8N_4, \tag{1.24}$$

where N is the total number of points in the causal set $\mathcal{C}$, and N_i is the number of $(i+1)$-element inclusive intervals in $\mathcal{C}$. This dependence on the dimension in a more fundamental

level should be removed.

Another proposal for gravitational action is presented in Refs. [30, 31], where they use the expanded volume of an Alexandrov neighborhood up to first order in curvature using RNC to derive an expression for the scalar curvature

$$R = \mathcal{L}_{\rm EH} = \frac{1}{D}\left\{\left(\frac{V(\tau)}{k_d\tau^d} - 1\right)\left(I_{d,0} + I_{d,1} + \tfrac{1}{4}k_d\right)\tau^d - \int\limits_{\alpha(p,q)}\left(\frac{V(p,x)}{k_d\tau^d(p,x)} - 1\right)\mathrm{d}^d x\right\}, \quad (1.25)$$

where k_d is the volume of a unit Alexandrov neighborhood of dimension d and height τ and

$$D = \left(\frac{d^2}{24(d+1)(d+2)} + \frac{d}{24(d+1)}I_{d,1}\right)\tau^{d+2} \quad (1.26)$$

$$I_{d,0} = \frac{1}{\tau^{d+2}}\int\limits_{\alpha_0}\left(x^0\right)^2\mathrm{d}^d r = \frac{k_d}{2(d+1)(d+2)} \quad (1.27)$$

$$I_{d,1} = \frac{1}{\tau^{d+2}}\int\limits_{\alpha_0}\left(x^1\right)^2\mathrm{d}^d r = \frac{(d-1)k_{d-1}}{8d(d+2)}\frac{\sqrt{\pi}\,\Gamma((1+d)/2)}{\Gamma(1+d/2)}. \quad (1.28)$$

One can discretize the action Eq. (1.25), by replacing τ with the discrete version $\kappa_d\ell$ where κ_d is a geometrical factor and $\ell = \rho^{-1/d}$ is the average distance between points determined by the density. One can write κ_d in terms of other known factors,

$$\kappa_d = \frac{k_{\max}}{\beta_d\left(k_d\right)^{1/d}}, \quad (1.29)$$

where $k_{\max}$ is the longest path connecting p and q, and β_d is the coefficient investigated by Brightwell and Gregory [24] and discussed in Eq (1.14),

$$\mathcal{R} = \frac{1}{\rho D}\left\{\left(\frac{N}{(k_{\max}/\beta_d)^d} - 1\right)\left(I_{d,0} + I_{d,1} + \tfrac{1}{4}k_d\right)\frac{(k_{\max}/\beta_d)^d}{k_d} - \right.$$
$$\left. - \sum_{p\prec x\prec q}\left(\frac{N(p,x)}{(k_{\max}(p,x)/\beta_d)^d} - 1\right)\right\}. \quad (1.30)$$

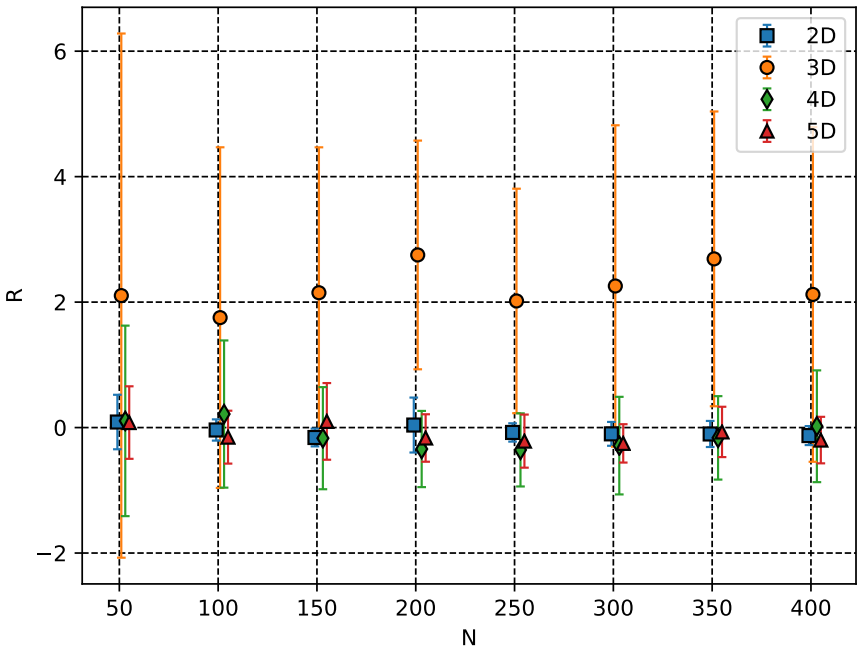

Figure 1.2. This figure shows the calculated average scalar curvature R over 25 sprinklings in Minkowski spacetime by approximating $\beta_d = 2$ using Sverdlov-Bombelli approach. The simulations are done for causal sets of sizes, 50, 100, ... but we have used small offsets for clearance.

This proposal is also dimension dependent and needs to be discretized in order for it to be applicable to causal sets. This is not yet doable at least until β_d is known exactly in Eq. (1.30). This expression is obtained by choosing a frame of reference which is not ideal in CST.

For a spacetime with a boundary, Dowker et al. [32] obtained an expression for discrete extrinsic scalar curvature from the boundary effects of a curved manifold on the volume of an Alexandrov neighborhood using RNC and Gaussian Normal Coordinates (GNC)

$$K = S^{(d)}_{\mathrm{CBT}}\left[\mathcal{C}, \mathcal{C}^-, \mathcal{C}^+; \vec{p}, \vec{q}\right] := \left(\frac{l}{l_p}\right)^{d-2} a_d \left(\sum_m p_m F_m\left[\mathcal{C}^-\right] + \sum_n q_n P_n\left[\mathcal{C}^+\right]\right), \tag{1.31}$$

with $\mathcal{C}^-$ the part of causal set in the past of the boundary and $\mathcal{C}^+$ is the part in the future, $F_k[\mathcal{C}]$ is the number of elements with k points to their future and $P_k[\mathcal{C}]$ is the number of elements with exactly k elements to their past excluding themselves, and

$$a_d = \frac{d(d+1)}{d+2}\left(\frac{c_{d-1}}{d(d-1)}\right)^{2/d}, \tag{1.32}$$

where $c_{d-1} = \pi^{d/2}/\Gamma(d/2+1)$ is the volume of a unit d-dimensional ball. In the continuum limit Eq. 1.31 reproduces the boundary term of the action that was previously introduced by Gibbons, Hawking and York [33, 34] if the coefficients p_m and q_m satisfy the following condition

$$\sum_{m=0} p_m \frac{\Gamma(\frac{1}{d}+m)}{m!} + \sum_{n=0} q_n \frac{\Gamma(\frac{1}{d}+n)}{n!} = 0, \tag{1.33}$$

$$\sum_{m=0} p_m \frac{\Gamma(\frac{2}{d}+m)}{m!} - \sum_{n=0} q_n \frac{\Gamma(\frac{2}{d}+n)}{n!} = 1, \tag{1.34}$$

where the values of m and n range up to the max number of layers used. As we can see there is a lot of freedom in choosing the parameters, but in the simplest case the action will be

just the difference between the number of past and future neighbors with $p_0 = 1/2 = -q_0$,

$$S_0^{(d)}\left[\mathcal{C}, \mathcal{C}^-, \mathcal{C}^+\right] := (l/l_p)^{d-2} \frac{a_d}{2\Gamma(2/d)} \left(F_0\left[\mathcal{C}^-\right] - P_0\left[\mathcal{C}^+\right]\right), \tag{1.35}$$

and then in addition to the above choice there are many different families of parameters p_m and q_n that would satisfy Eqs. (1.33) and (1.34).

Scalar Fields:

A scalar field of mass m in a causal set can be propagated, using propagators introduced in Refs. [35, 36], which for 2- and 4-dimensional causal sets, respectively, are given by

$$K_R^{(2)} := a^{(2)}\mathbf{R}\left(\mathbf{I} - a^{(2)}b^{(2)}\mathbf{R}\right)^{-1}, \quad a^{(2)} = \frac{1}{2}, \; b^{(2)} = -\frac{m^2}{\rho} \tag{1.36}$$

$$K_R^{(4)} := a^{(4)}\mathbf{L}\left(\mathbf{I} - a^{(4)}b^{(4)}\mathbf{L}\right)^{-1}, \quad a^{(4)} = \frac{\sqrt{\rho}}{2\pi\sqrt{6}}, \; b^{(4)} = -\frac{m^2}{\rho}, \tag{1.37}$$

where $\mathbf{I}$ is the Identity matrix, $\mathbf{R}$ is the Relations matrix, $\mathbf{L}$ is the Link matrix, and $a^{(d)}$ and $b^{(d)}$ are probabilities assigned to each element in the causal set, corresponding to processes that author calls "hopping" and "stopping" at each step as the field is propagating. The probabilities are chosen in such a way that in the continuum limit we obtain the regular Feynman propagator for scalar fields

$$G_{\mathrm{F}}^{(2)}(x) = \frac{1}{4}H_0^{(2)}(ms) \tag{1.38}$$

$$G_{\mathrm{F}}^{(4)} = \frac{1}{4\pi}\delta(s^2) - \frac{m}{8\pi s}H_1^{(2)}(ms), \tag{1.39}$$

where s is the proper spacetime distance and $H_i^{(2)}$ is the Hankel function of the second kind. As can be seen from Eqs. (1.36) and (1.37), the propagators are dimension-dependent. The two-dimensional propagator does depend on the spacetime separation between points in a way that reproduces well the continuum propagator even at low densities; however, in the

four dimensional case it only reproduces the continuum results in the limit that ρ approaches infinity.

Another approach to the same topic is presented in Ref. [30] where the authors choose a time frame and use the time axis of the Alexandrov neighborhood to define the derivatives in the Klein-Gordon equations

$$\partial_0\phi = \frac{\phi(q)-\phi(p)}{\tau} \tag{1.40}$$

$$\partial_k\phi\partial_k\phi = \frac{1}{I_{d,1}\tau^{d+2}}\int\limits_{\alpha(p,q)}(\phi(x)-\phi(p))^2\mathrm{d}^dx - \frac{I_{d,0}+\frac{1}{4}k_d}{I_{d,1}}\frac{(\phi(q)-\phi(p))^2}{\tau^2} \tag{1.41}$$

which leads to

$$\mathcal{L}_{\mathrm{KG}}(\prec,|g|,\phi;p,q) = \frac{3\left(\phi(q)-\phi(p)\right)^2}{\tau^2(p,q)} - \frac{360}{\pi\tau^6(p,q)}\int\limits_{\alpha(p,q)}\mathrm{d}^4x\left(\phi(x)-\phi(p)\right)^2 + \frac{1}{2}m^2\phi^2(p) \tag{1.42}$$

$$\mathcal{L}_{\mathrm{KG}}(\prec,|g|,\phi;x) = \lim_{\substack{p,q\to x\\ p\prec x\prec q}}\mathcal{L}_{\mathrm{KG}}(\prec,|g|,\phi;p,q) \Rightarrow S_{\mathrm{KG}} = \int\limits_{\mathcal{M}}\mathrm{d}^dx\sqrt{g}\mathcal{L}_{\mathrm{KG}}(\prec,|g|,\phi;x), \tag{1.43}$$

where $|g|$ is the determinant of the metric $g_\mu\nu$. The above equation requires discretization, which in turn also depends on the geometrical factor κ_d the same way it was shown in Eq. (1.25),

$$\begin{aligned}\mathcal{L}_{\mathrm{KG}}(\prec,|g|,\phi;x) &= \\ &= \left\{\left(1+\frac{I_{d,0}+\frac{1}{4}k_d}{I_{d,1}}\right)\left(\phi(q)-\phi(p)\right)^2 - \right. \\ &\quad \left. -\frac{k_d}{I_{d,1}(k_{\max}/\beta_d)^d}\sum_{p\prec x\prec q}\left(\phi(x)-\phi(p)\right)^2 - m^2\phi(p)^2\right\}\frac{(k_d\rho)^{2/d}}{(k_{\max}/\beta_d)^2}.\end{aligned} \tag{1.44}$$

1.3.3 Phenomenology

Every physics theory gets its credit from the phenomenology, i.e, if the experiments verify the predictions of the theory, it will get more acceptance in the scientific society. For quantum gravity the phenomenology, particularly looks less trivial, because the effects are

expected to be important at such small scales that direct observation is impossible.

In the case of CST, there are some phenomenological papers that focus on the indirect effects of the discreteness at larger scales. Here I only mention two of these results.

One of the impressive predictions of CST is the value of the Cosmological Constant Λ to the same order before it was measured by modern methods [37]. This particular calculation by Sorkin is based on a heuristic approach to the problem. Due to the Poisson distribution of spacetime atoms as it is assumed in CST, we would expect the number of points in a volume V to have some fluctuations

$$N \approx V \pm \sqrt{V}. \tag{1.45}$$

For a de Sitter spacetime with Λ as the scalar curvature, one can see from the Einstein-Hilbert action that Λ and V are conjugate of each other and in analogy to the time-energy uncertainty principle he writes

$$\Delta\Lambda\Delta V \sim \hbar. \tag{1.46}$$

Then, by using Eq. (1.45) and assuming that Λ is fluctuating about the average value of zero, one can deduce

$$\Lambda \sim V^{-1/2} \sim H^2. \tag{1.47}$$

Another interesting result was obtained by Dowker et al. [38] regarding the effect of discreteness on particles propagating in a causal set. Due to discrete nature of causal sets, if a particle wants to move on a causal set, it will not be able to follow the longest continuous path (the geodesic), but it will move along the closest possible path to a geodesic, which in analogy is taken to be the longest path in causal sets. This path will introduce some acceleration to the particle and one would expect to observe some effects in the larger scale.

To model this behavior the authors used a diffusion equation for the probability distribution $\rho(p^\mu, x^\mu, \tau)$, with p^μ, x^μ corresponding to the momentum and coordinate of

the particle respectively on the $\mathbb{H}^3 \times \mathbb{M}^4$ space, where the $\mathbb{H}^3$ represents the space of three independent components of 4-momentum (we are assuming the Lorentz invariance condition) and $\mathbb{M}^4$ is the Minkowski spacetime manifold

$$\frac{\partial \rho}{\partial \tau} = k\nabla_p^2 \rho - \frac{1}{mc^2} p^\mu \frac{\partial}{\partial x^\mu} \rho, \tag{1.48}$$

with τ the proper time, and k is the diffusion constant. For non relativistic particles in the laboratory or cosmic time, by choosing a hypersurface the equation reduces to

$$\frac{\partial \rho}{\partial t} = k\nabla^2 \rho, \tag{1.49}$$

which can be solved analytically with the solution

$$\rho = A(t) \exp\left(-\frac{p^2}{4kt}\right) \tag{1.50}$$

where $A(t)$ is a normalization factor. This solution very much resembles the Maxwell distribution, which suggests that even with the accelerating due to discreteness (or as the authors call it "swerves") the gas stays in thermal equilibrium, moreover it implies that the temperature changes linearly with time

$$\frac{\mathrm{d}T}{\mathrm{d}t} = \frac{2k}{mk_B}, \tag{1.51}$$

where k_B is the Boltzmann constant and T is the temperature. For the case of a proton, assuming that we have a millionth of a degree sensitivity, we find a bound on k

$$k \leq 10^{-56}\ \mathrm{kg^2 m^2 s^{-3}}.$$

According to the above one can heuristically calculate the maximum energy gain of a proton

due to discreteness according to $\langle E \rangle = 3k_{\mathrm{B}}T/2$

$$\frac{\langle \Delta E \rangle}{\Delta t} = 4.3 \times 10^{-11} eV/s. \tag{1.52}$$

This very simplified calculation results into an effect that can not explain the high energy cosmic rays, as at this rate it will take more than the age of the universe to even double the energy of protons in such. More modification of the model, including making k a function of the local factors such as the density of particles is needed, which if k is high enough it might reduce the diffusion rate.

CHAPTER 2

ALGORITHMS

In this chapter I present a general picture of the way the sprinklings are done in my simulations and how I obtained the results.

As was discussed in the previous chapters, only causal sets whose elements are uniformly distributed in a manifold are considered as faithfully embedded causal sets and therefore manifoldlike. It was also discussed that such a causal set can be obtained by randomly generating points in an already existing manifold. The way that the points are generated has special importance. Usually in a causal set theory most of the calculations are done in an Alexandrov neighborhood, because they have a finite volume and effects of the edges of the boundaries are avoided. One can obtain a uniform distribution of points by randomly generating the values of coordinate. In such a case one needs to choose a box of dimension d and randomly generate numbers for coordinates in that box and reject the points that are not in the Alexandrov neighborhood which is contained in the box. The time complexity of this method is exponential. It is also possible to come up with a procedure that does not use the rejection process and for that in an arbitrary dimension d one requires to use the spherical coordinate $r = \sqrt{\sum_{i=1}^{d-1} x_i^2}$ and time t, and the convert them to null coordinates $u = (t + r)/\sqrt{2}$ and $v = (t - r)/\sqrt{2}$, and regular angular coordinates θ_i based on the number of dimensions. Using this method one can directly sprinkle the points inside the Alexandrov neighborhood. In all the computational parts of this dissertation , I have used the rejection method because for the number of points in consideration the time that is saved is negligible. This process is doable with arbitrary dimensional Minkowski space, de Sitter space and Friedmann-Lemaître-Robertson-Walker (FLRW). For the other spacetimes

it might be possible but maybe through some numerical calculations which are necessary to determine the light cone boundaries and measurements of distance.

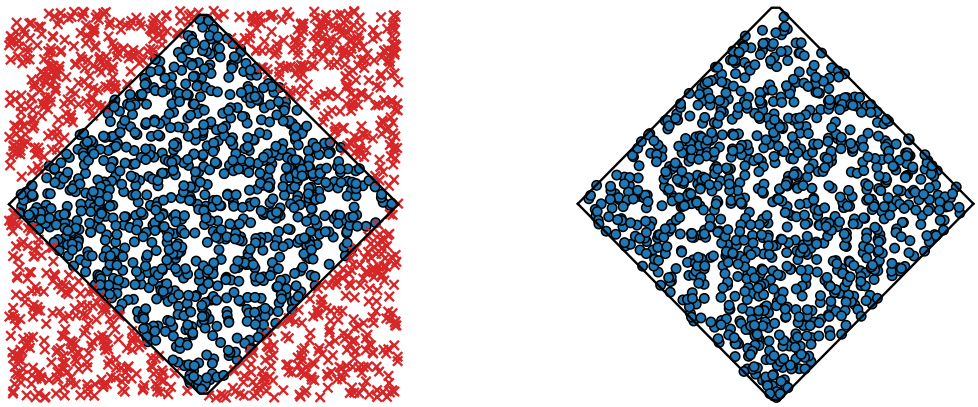

Figure 2.1. (Left) Sprinkling of points in a square by rejection. (Right) Sprinkling without rejection in the Alexandrov neighborhood. In both cases the Alexandrov neighborhood contains 1000 points.

The Relations matrix is obtained by only looking for the condition that the points are causally related, with the consideration that value 1 is assigned to the ijth element if and only if $p_i \prec p_j$. The Links matrix can be created with the same method except with an extra condition that the points are nearest neighbors. Time complexity for finding the Link and Relation matrices are $\mathcal{O}(N^2)$[60].

CHAPTER 3

PATH LENGTH DISTRIBUTION IN CAUSAL SETS

3.1 The Path Length Distribution

In this section we will derive an expression for the distribution of maximal-chain lengths in a causal set sprinkled uniformly at random in an Alexandrov neighborhood $\mathcal{A}(p,q)$ of d-dimensional Minkowski spacetime, and show the results of some numerical simulations. This distribution provides a good opportunity for statistical analysis of properties of the causal set. We will refer to an element of such a sprinkling that is contained in some smaller region within $\mathcal{A}(p,q)$ simply as a point in that region, and we will call a region empty if it does not contain any of the randomly distributed points. A maximal chain of length k between points x_1 and x_{k+1} is defined such that for each i the Alexandrov neighborhood $\mathcal{A}_{i,i+1} = \mathcal{A}(x_i, x_{i+1})$ is empty; i.e., $x_i \prec\!\!* \, x_{i+1}$ in the causal set.

The number of k-paths between two points $p = x_1$ and $q = x_{k+1}$ in a causal set uniformly embedded in Minkowski space is a random variable, whose mean value can be evaluated analytically by picking $k-1$ possible locations for the other x_i, calculating the probability that one causal set point is found in each infinitesimal neighborhood $\mathrm{d}x_i$ and each Alexandrov neighborhood $\mathcal{A}_{i,i+1}$ is empty, and integrating over all the x_i.

As was discussed before, the probability distribution of fixed N points in a volume V_0 is binomial and for the case of very small volumes inside V_0, the Poisson distribution might be a good approximation. However, a recent study has shown that even in the case of an infinitesimal $\mathrm{d}x_i$, this probability cannot directly be approximated by a Poisson distribution of constant density $\rho = N/V_0$ and it needs some modification specially in the case of longer chains and paths. Thus, for each of the $\mathrm{d}^d x_i$ the probability that it contains exactly one point

will not be totally independent, and it can be written as $\rho\delta V \mathrm{e}^{-\rho\delta V} = \rho_i \,\mathrm{d}^d x_i \,\mathrm{e}^{-\rho_i \,\mathrm{d}^d x_i} \approx \rho_i \,\mathrm{d}^d x_i$ where the density ρ_i depends on i. Those probabilities can be considered to be independent only in the cases that the number of links in the chain/path is much much smaller than the total number of points, $k \ll N$. The intervals $I_{i,i+1}$ however may not be small, and for those we will use the binomial distribution. In particular, the probability that a region of volume V is empty is given by $P_0 = (1 - V/V_0)^N$, and for the union $\mathcal{A}_{1,2} \cup \cdots \cup \mathcal{A}_{k,k+1}$ of all Alexandrov neighborhoods between pairs of points that probability can be written as

$$P_0 = \left(1 - \frac{\sum_{i=1}^{k} V_{i,i+1}}{V_0}\right)^{N-k+1} . \tag{3.1}$$

Putting these together we then get, following the same approach as in Ref. [23] but with the corrected densities discussed in Ref. [39],

$$P(x_2, \ldots, x_k)\,\mathrm{d}^d x_2 \cdots \mathrm{d}^d x_k = \tfrac{N}{V_0}\,\mathrm{d}^d x_2 \cdots \tfrac{N-k+2}{V_0}\mathrm{d}^d x_k \left(1 - \tfrac{\sum_i^k V_{i,i+1}}{V_0}\right)^{N-k+1} + \mathcal{O}\big((\mathrm{d}^d x)^2\big) \tag{3.2}$$

We now identify the probability in Eq. 3.2 with the mean number of paths through those locations, which integrated over all x_i gives the mean number of k-paths between p and q,

$$\langle n_k^{(d)} \rangle = \frac{N!}{(N-k+1)! V_0^{k-1}} \int\limits_{\mathcal{A}_1} \mathrm{d}^d x_2 \cdots \int\limits_{\mathcal{A}_{k-1}} \mathrm{d}^d x_k \left(1 - \frac{\sum_i^k V_{i,i+1}}{V_0}\right)^{N-k+1} , \tag{3.3}$$

where $\mathcal{A} = \mathcal{A}(x_i, q)$ is the Alexandrov neighborhood between x_i and the maximal element q in the manifold; for simplicity, from now on we will drop the angle brackets, $\langle n_k \rangle \mapsto n_k$. Using the binomial expansion we can write

$$\begin{aligned} n_k^{(d)} = \frac{N!}{(N-k+1)! V_0^{k-1}} \sum_{i_1=0}^{N-k+1} \binom{N-k+1}{i_1} \left(-\frac{1}{V_0}\right)^{i_1} \times \\ \sum_{i_2=0}^{i_1} \binom{i_1}{i_2} \cdots \sum_{i_k=0}^{i_{k-1}} \binom{i_{k-1}}{i_k} \int\limits_{\mathcal{A}_1} \mathrm{d}^d x_2 \cdots \int\limits_{\mathcal{A}_{k-1}} \mathrm{d}^d x_k \, (V_{12})^{i_1 - i_2} \cdots (V_{k,k+1})^{i_k} . \end{aligned} \tag{3.4}$$

3.1.1 Two Dimensions

In two dimensions the volume of an Alexandrov neighborhood can be easily calculated using the null coordinates

$$u = (t + x)/\sqrt{2}\,, \qquad v = (t - x)/\sqrt{2}\,, \tag{3.5}$$

in terms of which

$$V_{i+1,i} = (u_{i+1} - u_i)(v_{i+1} - v_i)\,. \tag{3.6}$$

With these expressions for the volumes, in the $d = 2$ case the integrals in Eq. (3.4) give

$$n_k^{(2)} = \frac{N!}{(N-k+1)!} \sum_{i=0}^{N-k+1} \binom{N-k+1}{i} (-1)^i \frac{\Gamma(i+1)}{\Gamma(i+k)^2}\, f_{i,k}^{(2)} \tag{3.7}$$

where we used $N = \rho V_0$ and

$$f_{i,k}^{(2)} = \sum_{i_2=0}^{i} \Gamma(1+i-i_2) \times \underbrace{\times \sum_{i_3=0}^{i_2} \Gamma(1+i_2-i_3) \cdots \underbrace{\sum_{i_{k-1}=0}^{i_{k-2}} \Gamma(1+i_{k-2}-i_{k-1}) \underbrace{\sum_{i_k=0}^{i_{k-1}} \Gamma(1+i_{k-1}-i_k)\,\Gamma(i_k+1)}_{f^{(2)}_{i_{k-1},2}}}_{f^{(2)}_{i_{k-2},3}}}_{f^{(2)}_{i_2,k-1}} \,. \tag{3.8}$$

As suggested by the underbraces, this definition implies the recursion relation

$$f_{i,k}^{(2)} = \sum_{j=0}^{i} \Gamma(1+i-j) f_{j,k-1}^{(2)}\,, \tag{3.9}$$

with $f_{i,1}^{(2)} := \Gamma(i+1)$. Using Eqs. (3.7)–(3.9), n_k may now be calculated for any N and k.

3.1.2 d dimensions

For the general d dimensional case, we redefine the null coordinates in the following way

$$u_{ij} = (\Delta t_{ij} + \Delta r_{ij})/\sqrt{2}\,, \qquad v_{ij} = (\Delta t_{ij} - \Delta r_{ij})/\sqrt{2}\,, \tag{3.10}$$

where $r_{ij} = \sqrt{\sum_{\ell=1}^{d-1}(\Delta x_{ij}^{\ell})^2}$, in terms of which $V_{i+1,i}$, a d-dimensional double cone of height $\Delta\tau_{i+1,i}$, is

$$V_{i+1,i} = k_d \left(u_{i+1,i} v_{i+1,i}\right)^{d/2}\,, \tag{3.11}$$

$$k_d = \frac{\pi^{(d-1)/2}}{d(d-1)\Gamma((d-1)/2)2^{d-2}}. \tag{3.12}$$

Solving the integral, we find a generalization of the results in Eq. (3.7) which by setting $d = 2$ reduces to the previous result. This equation can be written in the form

$$\begin{aligned} n_k^{(d)} = {} & \frac{N!}{(N-k+1)!}\left(\frac{\Gamma(d+1)}{2\Gamma(d/2)}\right)^{k-1} \times \\ & \times \sum_{i_1=0}^{N-k+1} \binom{N-k+1}{i_1} (-1)^i \frac{\Gamma(i_1+1)}{\Gamma((i_1+k)d/2)\Gamma(1+(k-1)d/2+i_1 d/2)} \times \\ & \times \sum_{i_2=0}^{i_1} \frac{\Gamma((i_1-i_2+1)d/2)\Gamma(1+(i_1-i_2)d/2)}{\Gamma(i_1-i_2+1)} \times \cdots \times \\ & \times \sum_{i_k=0}^{i_{k-1}} \frac{\Gamma((i_{k-1}-i_k+1)d/2)\Gamma(1+(i_{k-1}-i_k)d/2)}{\Gamma(i_{k-1}-i_k+1)} \frac{\Gamma((i_k+1)d/2)\Gamma(1+i_k d/2)}{\Gamma(i_k+1)} \end{aligned} \tag{3.13}$$

An alternative rearrangement of the formula in a more compact notation gives

$$\begin{aligned} n_k^{(d)} = {} & \frac{N!}{(N-k+1)!}\left(\frac{\Gamma(d+1)}{2\Gamma(d/2)}\right)^{k-1} \times \\ & \times \sum_{i=0}^{N-k+1} \binom{N-k+1}{i} \frac{(-1)^i \Gamma(i+1)}{\Gamma((i+k)d/2)\Gamma(1+(k-1+i)d/2)} f_{i,k}^{(d)}, \end{aligned} \tag{3.14}$$

where the $f_{i,k}^{(d)}$ satisfy the following recursion relation

$$f_{i,k}^{(d)} = \sum_{j=0}^{i} \frac{\Gamma((i-j+1)d/2)\Gamma(1+(i-j)d/2)}{\Gamma(i-j+1)} f_{j,k-1}^{(d)}, \tag{3.15}$$

with

$$f_{i,1}^{(d)} = \frac{\Gamma((i+1)d/2)\Gamma(1+id/2)}{\Gamma(i+1)}. \tag{3.16}$$

With some algebra we can see that by setting $d = 2$ the results reduce to what had already been described for two dimensions, and by setting $i = 0$ we reproduce the result by Meyer, explained in Ref. [23] on the chain length distribution between the minimal and maximal points, with a modified density

$$\begin{aligned} c_k^{(d)} &= \frac{N!}{(N-k+1)!} \left(\frac{\Gamma(d+1)}{2\Gamma(d/2)} \right)^{k-1} \frac{\Gamma(\frac{d}{2})}{\Gamma(k\ d/2)\Gamma(1+(k-1)d/2)} = \\ &= \frac{N!}{(N-k+1)!} \frac{1}{k-1} \left(\frac{\Gamma(d+1)}{2} \right)^{k-2} \frac{\Gamma(d)\Gamma(\frac{d}{2})}{\Gamma(k\frac{d}{2})\Gamma((k-1)\frac{d}{2})}. \end{aligned} \tag{3.17}$$

3.2 Results of Simulations

We wish to compare the results of the analytical distribution with values obtained from actual manifoldlike causal sets generated from numerical simulations of random sets of points sprinkled with uniform density in the Alexandrov neighborhood defined by two timelike related points in Minkowski space. From Fig. 3.1 it's easy to see that the theory matches well with the average of the simulations, though it is worth pointing out that as the large error bars suggest, individual sprinklings can deviate significantly from the theory. This problem can be somewhat though not completely mitigated by considering only the peak and width[1] of the distribution rather than its entirety. The shape of these distributions is nearly Gaussian, allowing us to characterize each curve with just these two numbers. As one can see in Fig. 3.2 the relative errors in both the peak position and the width decrease with

[1]By width we mean full width at half maximum.

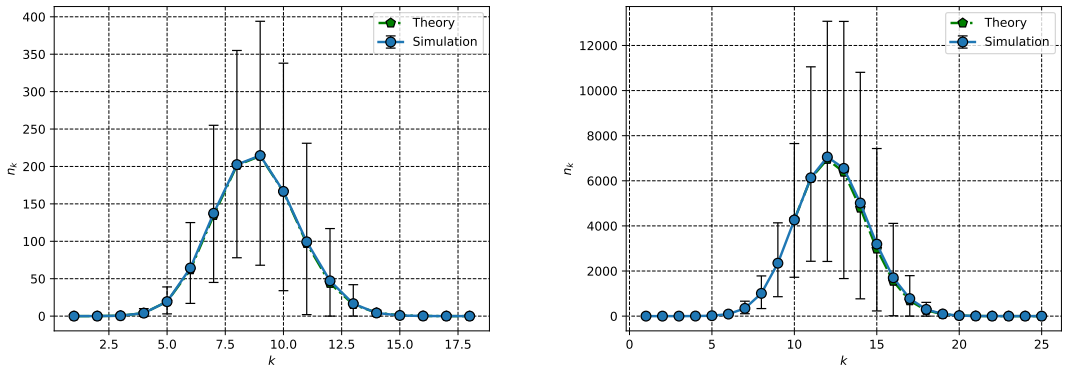

Figure 3.1. A comparison of the average of many sprinklings of 50 and 100 points on a two-dimensional Minkowski manifold, to their corresponding analytical distributions, on the left and right respectively. Due to numerical error caused by the alternating sign of the sum in Eq. (3.7) and the large numbers for less than $k = 9$, the theory curve starts at 9.

N, implying that the larger errors in Fig. 3.1 are primarily due to fluctuations in the total number of paths rather than the shape of the curve considered as a probability distribution; however, there is still enough error in the peak and width to cause us some concern. As a result, any application based on this distribution should account for statistical fluctuations in evaluating a single causal set. For instance, if one wishes to use this distribution for its stated purpose of determining manifoldlikeness of causal sets, the failure of a particular causal set to exactly match either the full analytical distribution or its peak and width should *not* be taken as a sign that the causal set is not manifoldlike; rather, a fairly large range around the analytical distribution should be used, and causal sets which fall into this range should be considered candidates for manifoldlike causal sets. We will discuss this further in the next section.

3.3 Manifoldlike Causal Sets

One of the original motivations for this work was to explore the possibility of using the mean path length between two causal set elements p and q for a known value for the volume of $\mathcal{A}(p, q)$ as a dimension estimator, similar to the use of the longest path length in Ref. [23], with the possible computational advantage that sampling the set of paths between

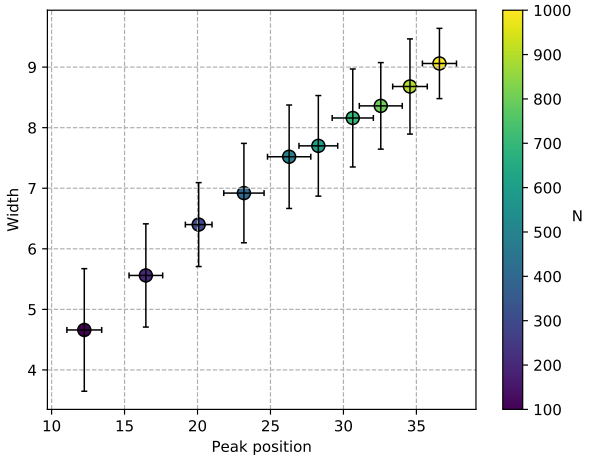

Figure 3.2. A plot of width vs peak position for a variety of sizes of sprinkled causal sets. The color indicates the number N of elements in the causal set.

p and q and using an average length to estimate the mean may be easier than finding the longest path. From simulations in Minkowski space of higher-dimensionalities, it appears that the average length of a sample of a few paths is indeed a valid dimension estimator, though it is unclear whether it is computationally better than the longest path method. One benefit of our approach and similar ones using the distribution of path lengths, however, is that it provides a criterion of manifoldikeness for causal sets.

It is clear even from simple examples that quantities like the longest or the mean path length may be good dimension estimators only for causal sets known to be manifoldlike, and do not by themselves distinguish those causal sets from non-manifoldlike ones. For example, the union of m chains of length k with minimal points and maximal points identified is a causal set that can always be embedded in 2D Minkowski space, but adjusting the values of m and k one can obtain a relationship between the total number of elements $N = m(k-1)+2$ and the longest or mean path length k that reproduces that of any Minkowski dimensionality. Similarly, a causal set could be constructed as the union of separate paths of various lengths all sharing the same minimal and maximal element, and with no other overlap, as in the left side of Fig. 3.3, with the number of chains of each length adjusted in a way that exactly

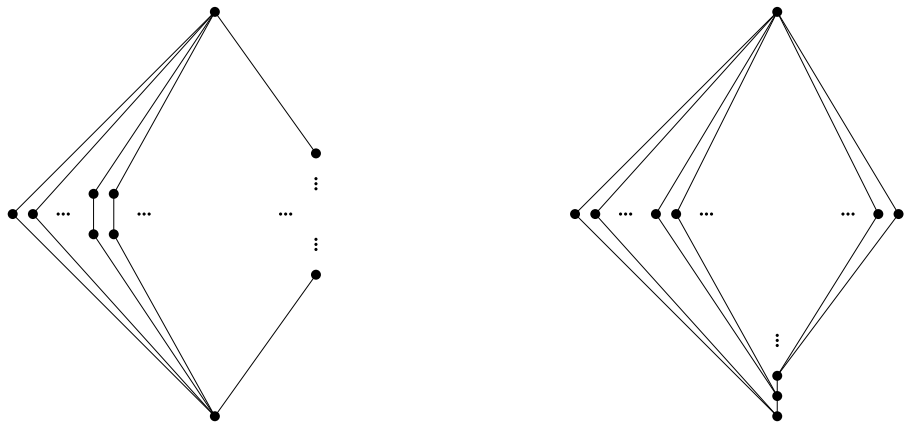

Figure 3.3. (Left) An artificially produced causal set whose purpose is to mimic both the height and width of our path length distribution. (Right) A similarly produced artificial causal set which eliminates some redundancies to reduce the number of points while maintaining the path length distribution; however, it still has far more points than its manifoldlike cohorts.

matches the mean and width of the typical manifoldlike distribution. However, while the construction would yield the right value of n_k for any length k, the total number of points in the causal set, $N = \sum_{k=2}^{k_{\max}} n_k(k-1) + 2$, would be quite different as the manifoldlike distribution would have many paths sharing points and this contrived example does not. We could make the example slightly more realistic by forcing the paths to share all points not linked to the maximum point as in the right side of Fig. 3.3. This would limit the number of points significantly, with a total of $N = \sum_{k=2}^{k_{\max}} n_k + k_{\max}$, where $k_{\max}$ is the length of the longest path in the causal set. However, for $N \gg 1$ this may still have several orders of magnitude more points than a manifoldlike causal set, as we can see by considering for example the right side of Fig. 3.1. If we use the average values of these 100-point sprinklings, the first method requires around 4×10^5 points while the second one requires around 4×10^4 points.

What we propose as a first manifoldlikeness criterion based on the distribution of path lengths n_k is simply that any N-element causal set for which the mean value k_0 and the width Δ of that distribution are not consistent with the corresponding theoretical values within statistical fluctuations cannot be manifoldlike. Based on the few examples we just saw,

finding nonmanifoldlike causal sets that satisfy this condition is not trivial. Nevertheless, this condition is most likely not a sufficient one for manifoldlikeness. To further explore which causal sets meet or do not meet our criterion we will now provide two other types of examples of nonmanifoldlike causal sets.

One type includes causal sets that are not manifoldlike but are interesting for other reasons, and fail our criterion. The first example is a causal set that has one maximal and one minimal element, with all other elements located between them and unrelated to each other (i.e., one large antichain with added minimal and maximal elements); the path length distribution is a Kronecker delta $n_k = \delta_{k,2}$, with a sharp peak at length 2 and zero for other lengths. A regular "diamond lattice" (shown in the left side of Fig. 3.4) also has a path distribution sharply peaked at some length $k_0 \approx \sqrt{N}$, with no paths of other lengths. More generally, most randomly chosen causal sets of N elements with $N \gg 1$ will look like the 3-layer Kleitman and Rothschild limit [16] shown in the right side of Fig. 3.4, in which the first and third layers have $N/4$ elements, each of which is related to about half of the $N/2$ elements in the second layer; for such a causal set again $n_k = \delta_{k,2}$. The causal sets in these examples are all nonmanifoldlike, as one would not obtain them from uniform distributions of points in a Lorentzian manifold. The KR is clearly not a uniform distribution, but in the case of the square lattice it should be noted that the distribution might only appear to be uniform in the frame in which the causal set looks like a square lattice, and it will clearly not be uniform in a boosted frame.

The other type of examples includes causal sets that are still not manifoldlike, but are likely to meet our criterion for manifoldlikeness. Fig. 3.5 shows the effect of adding one extra point to a causal set obtained from a 250-point random sprinkling in an Alexandrov neighborhood $\mathcal{A}(p, q)$ of 2D Minkowski space. The added point was to the future of a point approximately in the middle of the sprinkled causal set, and linked directly to the maximal element q; the left side of the figure shows the resulting augmented causal set. Because the added point gives rise to additional paths which are shorter than the ones that go through

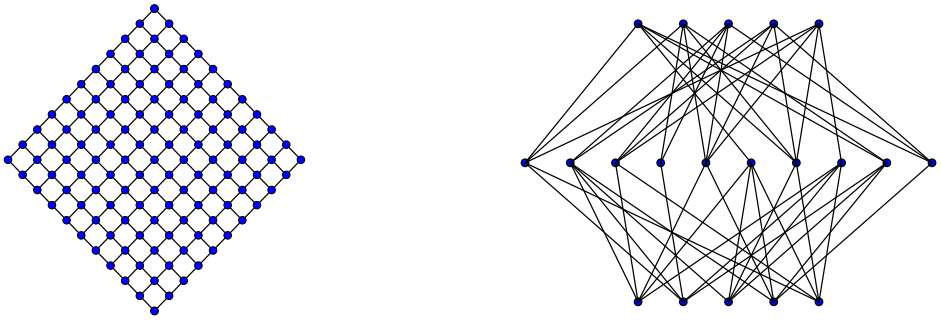

Figure 3.4. (Left) A regular lattice of $11^2 = 121$ points. The path distribution for this set is also sharply peaked, at $k = 20$ in this case, and not at all similar to that of a causal set from a random distribution of spacetime points. (Right) A 20-element causal set illustrating the Kleitman-Rothschild limit, which has a sharp peak for path length $k = 2$.

the original, sprinkled causal set, the new path length distribution will exhibit an additional small bump with a peak length shorter than the overall k_0. The right side of the figure shows the difference between the new path length distribution and the one without the additional point. This difference is very small compared to the overall distribution, but the feature it shows may be identifiable as characteristic of this particular type of nonmanifoldlike causal set.

The relationship between the above criterion for manifoldlikeness and different ways in which a causal set may fail to be manifoldlike, helps us to establish which additional criteria are needed to exclude nonmanifoldlike causal sets that are not physically interesting. It may possibly also help us formulate a more quantitative way to take into account statistical fluctuations in the path length distribution that would allow us to include causal sets which, strictly speaking, are not faithfully embeddable in a Lorentzian manifold, but may be physically interesting and we may want to call manifoldlike (see, e.g., Ref. [42]).

The above results help us set up a procedure to establish whether a causal set is close to a spacetime manifold and address one of the most fundamental questions in causal set theory. The results for higher dimensions may have other applications, for instance in the

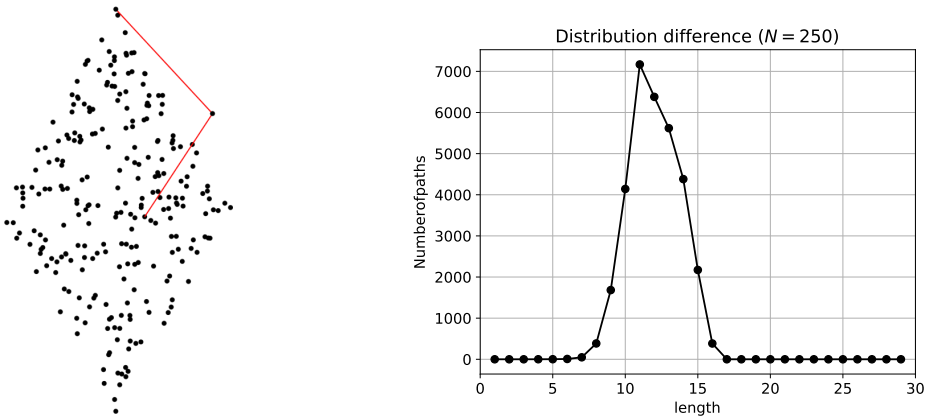

Figure 3.5. Left: Causal set obtained from sprinkling in 2D Minkowski space and one added point with "non-local" links. Right: Difference between the path length distributions.

expression for the Green's function for scalar fields propagating on causal sets in 4 dimensions [48]. Last but not least, these results establish a relation between the most probable path length and the proper time in the continuum, which can be used to discretize the action written in Refs. [30, 31] and was not known in general.

3.4 Curved Spacetimes

A good measure for manifoldlikeness is one that can distinguish manifoldlike causal sets regardless of the type of manifold that the causal set is embedded in. In this section I will present a preliminary result of the parameter space (width and peak of the path length distribution) for a causal set that is obtained from Poisson sprinkling in a de Sitter spacetime and then further expand on how the criterion could be used in an action in chapter 6.

As seen from Fig. (3.6), the two spacetimes remain almost indistinguishable up to at least $N = 1000$ and therefore this criterion does not seem to exclude a simple curved spacetime like de Sitter. In general the total distribution of paths in a Minkowski space is does deviate from the distribution in the de Sitter space, but using the while distribution is not very convenient, specially as the number of points increases.

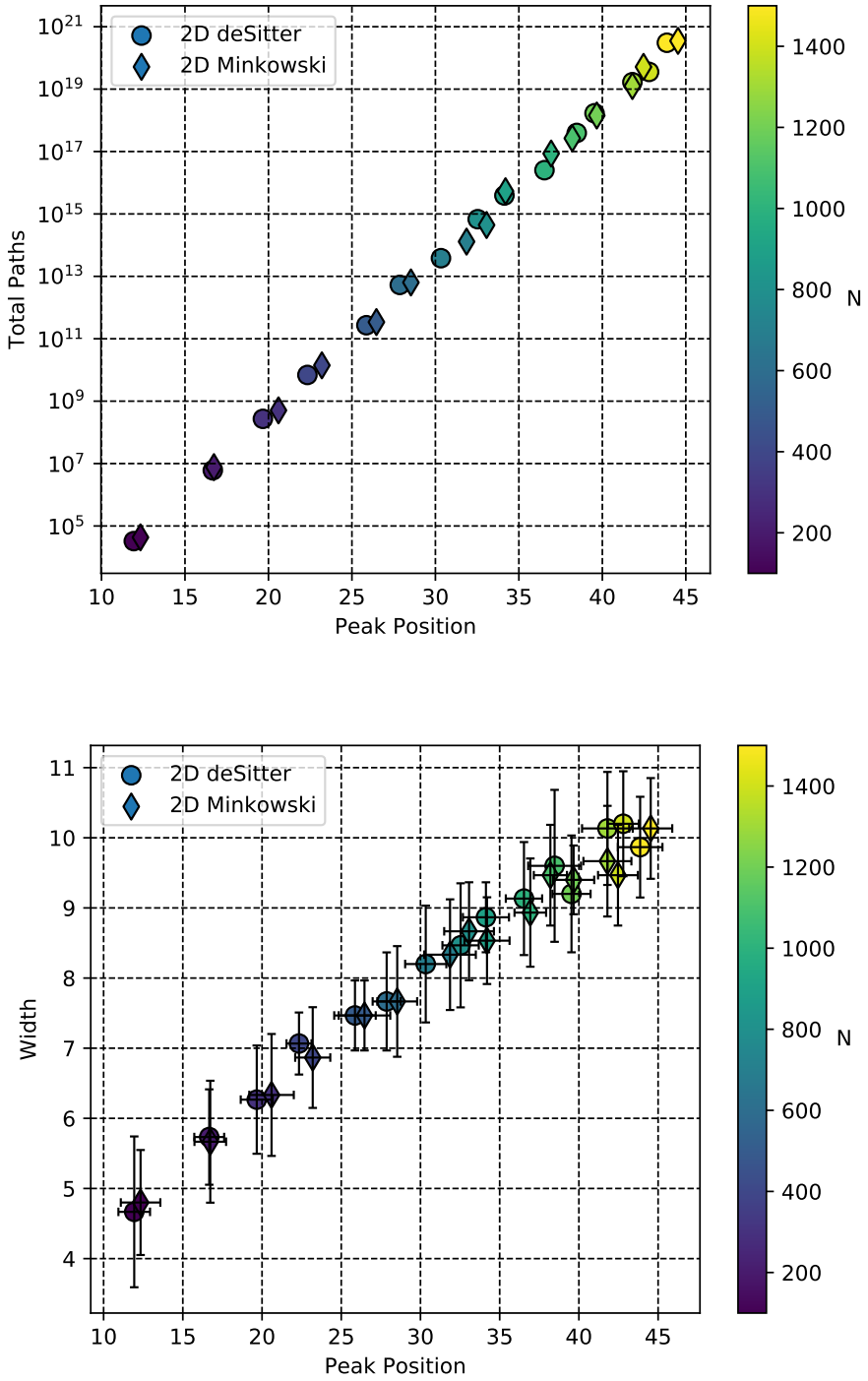

Figure 3.6. The parameter space for 2-dimensional causal sets embedded in Minkowski and de Sitter manifolds, for $N \in [100, 1500]$. In both cases the density is held fixed, because for the sake of comparison of two different spacetimes, the same density is equivalent to using the same length scale in both spacetimes. Up to $N = 1000$ points there is not a significant difference between the two spacetimes.

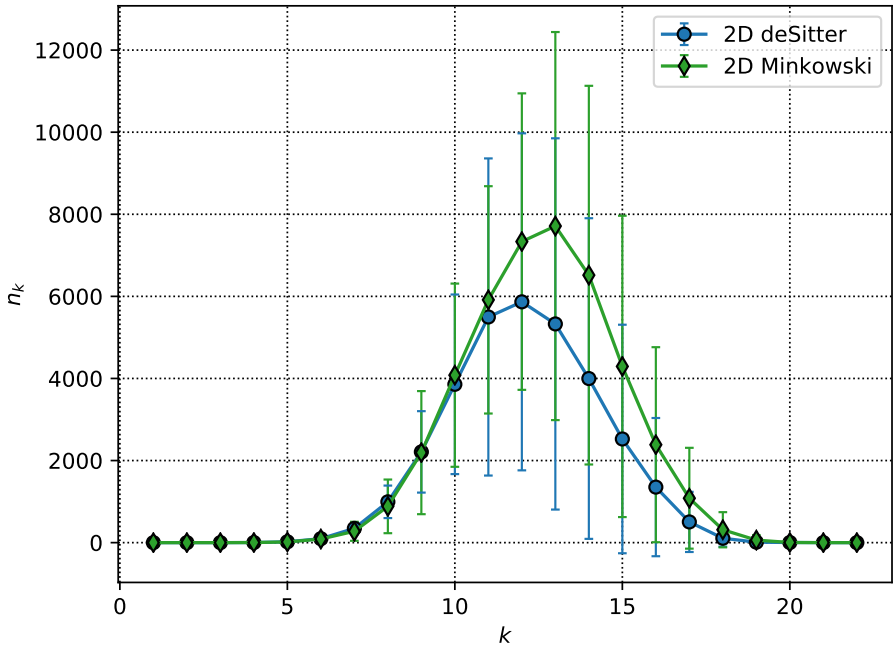

Figure 3.7. The path length distribution of causal sets embedded in Minkowski and de Sitter spacetimes, with the same density, with values of Hubble-Lemaître parameter $H = 10^4/N^{1/d}$

CHAPTER 4

DIMENSION OF CAUSAL SETS

4.1 Average Path Length

A causal set that is embeddable in Minkowski spacetime can be obtained by constructing it as already embedded in Minkowski manifold from sprinkling points at random with uniform density through a Poisson process on it [18]. If one then considers that causal set as an abstract one, and studies it as a way to get information on properties of embeddable causal sets, one of the quantities that one is interested in obtaining from the causal set is the dimension of the manifold that it is obtained from. To find any physical quantity in CST, one needs to use some invariant quantity obtained from the causal set, e.g., the distribution of Alexandrov neighborhoods, distributions of chains, etc. I use paths to obtain the dimension because it resembles the spectral dimension which is the usual method used in other approaches to quantum gravity such as CDT [49]. Because of the bell-shaped distribution of the path length distribution the initial motivation was to use a few sample of paths at random to approximate the actual value of the average path length which can be calculated by the following numerical algorithm

$$\bar{k} = \frac{1}{n_{\rm sp} \times n_{\rm sa}} \sum_{i=1}^{n_{\rm sp}} \sum_{j=1}^{n_{\rm sa}} \ell_j^{(i)}, \tag{4.1}$$

where $n_{\rm sp}$ is the number of sprinklings, $n_{\rm sa}$ is the number of samples and $\ell_j^{(i)}$ is length of the jth sample in the ith sprinkling.

However, to choose the paths at random one needs to assign a weight to each next possible step which is equal to the number of paths to the future of that point. This

means that in order to have the precise value for the weights we actually need to know that total distribution of the paths and therefore taking the paths at random will not be any cheaper computationally as we thought. Therefore for the rest of this section I abandon the approximated average and use the actual average obtained from the distribution.

4.2 Dimension

The approach we proposed in [49] to estimating the Minkowski dimension of a poset is based on the distribution of path lengths in it. Examples of such distributions are shown in figure 4.1 for posets obtained from Minkowski space sprinklings. In these examples the curves are bell-shaped, with an average length $\bar{k}$ and full width at half maximum Δ that differ for different values of d; if the number of points is kept constant, as the dimension increases both $\bar{k}$ and Δ tend to smaller values because of the extra volume introduced by the extra dimensions; the shape of the distribution however remains the same for all dimensions. When estimating d, this encourages us to use the average path length $\bar{k}$, as a quantity that may be subject to smaller statistical fluctuations than $k_{\max}$.

The average path length in a poset sprinkled in Minkowski space can be numerically calculated as follows. We first find the total number of k-element paths n_k and the total number of paths N_{paths} between the minimal element p_0 and the maximal element p_{N+1} using the link matrix,

$$n_k = (L^k)_{0,N+1} \ , \qquad N_{\text{paths}} = \sum_{k=1}^{N+1} n_k \ . \tag{4.2}$$

Notice that $N+1$ is the longest possible path length (in fact, $k = N+1$ is only achieved when the poset is totally ordered), but in practice in a simulation the summation for N_{paths} can be stopped after $k = l$ if it is found that $(L^l)_{ij} = 0$ for all (i, j). Using these quantities, the average path length can then be found simply as

$$\bar{k} = \frac{1}{N_{\text{paths}}} \sum_{k=1}^{N+1} k \, n_k \ . \tag{4.3}$$

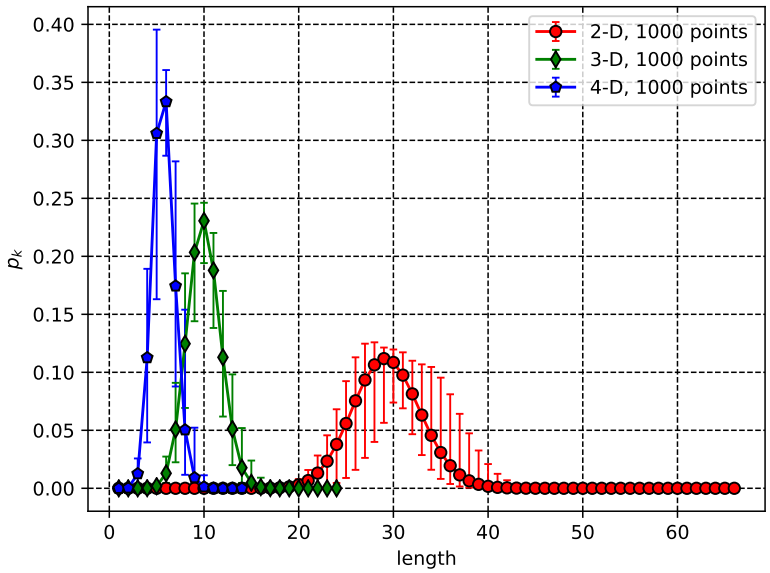

Figure 4.1. The probability distribution of path lengths for various dimensionalities and $N = 1000$ points. The "error bars" indicate the largest and smallest value obtained for n_k in the 50 sprinklings generated for each pair of values of d and k.

As for $k_{\max}$ in the Brightwell-Gregory approach, in the large-N limit the average path length in any given number of dimensions will be proportional to $N^{1/d}$, so we can write down an analogous relation between $\bar{k}$ and N, of the form

$$\bar{k} = \alpha_{d,N}\, N^{1/d} \,. \tag{4.4}$$

An interesting aspect of our approach is that it is in fact possible in principle to numerically calculate exact values for $\alpha_{d,N}$ [49]. We could then rewrite (4.4) as

$$d = \frac{\ln(N)}{\ln(\bar{k}/\alpha_{d,N})} \,, \tag{4.5}$$

and, using the theoretically derived values of $\alpha_{d,N}$, find the d that solves (4.5) exactly, at least in principle and again possibly using numerical methods. The problem is that the

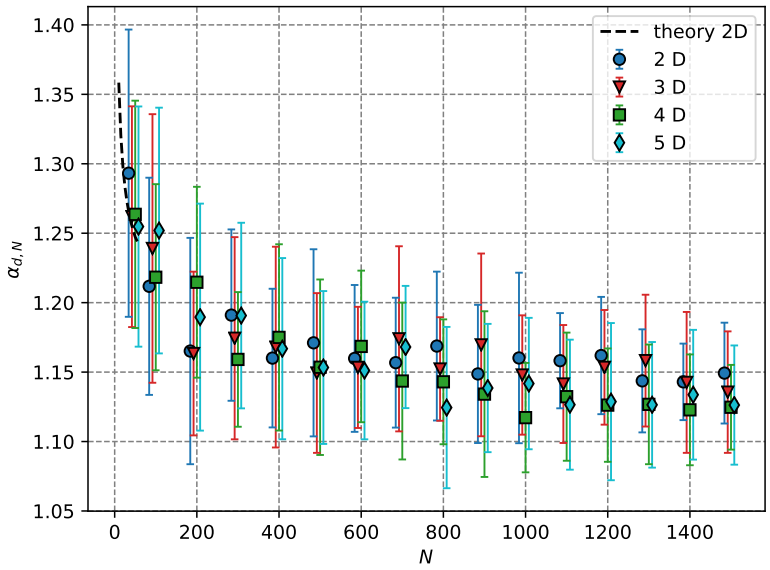

Figure 4.2. The value of $\alpha_{d,N}$ for various dimensionalities as a function of N. The error bars indicate the standard deviation of the results obtained from 15 sprinklings for each d and N. The dashed line indicates the analytically calculated values for $d = 2$ and $N \leq 55$. The simulations are done for causal sets of sizes, 50, 100, ... but we have used small offsets for clearance.

size of the numbers used to calculate those exact values is a fast growing function of N. For $d = 2$ we have only calculated the exact $\alpha_{d,N}$ up to $N = 55$. Figure 4.2 shows those values (dashed line), together with approximate values estimated using 15 Minkowski space sprinklings in $d = 2, 3, 4, 5$ and various values of N up to 1500. The error bars shown indicate the standard deviation of the results obtained from the 15 sprinklings generated for each d and N, and are mostly due to statistical fluctuations in the value of the average $\bar{k}$. (For reference, the computing time for each 1000-point sprinkling with $d = 2$ on a regular laptop computer with a 2.3-GHz Intel Core i5 processor is less than a minute, a number that can be better appreciated if we consider that the total number of paths in the resulting poset is $N_{\text{paths}} \approx 3 \times 10^{16}$.)

An interesting observation is that, based on figure 4.2, $\alpha_{d,N}$ appears to be very weakly dimension dependent and if we define $\alpha_N \equiv \alpha_{d,N}$, then α_N appears to tend to the asymptotic

value of 1.15 for large values of N. The dimension estimates for the posets generated with the above values for d and N are shown in figure 4.3. For reasons similar to the ones explained in Section 1.3.1 for the Brightwell-Gregory approach, the value of α we used in (4.5) to estimate d was 1.15 for all (d, N).

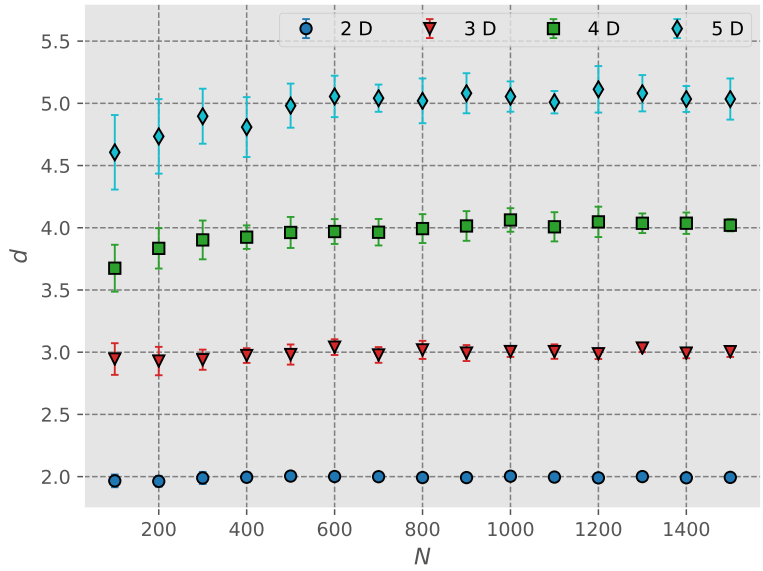

Figure 4.3. The estimated dimension of Minkowski space calculated using the average path length approach from simulations in $d = 2$, 3, 4 and 5 dimensions as a function of N. The error bars indicate the standard deviation of the results obtained from 15 sprinklings generated for each d and N.

4.3 Comparison with Other Dimension Estimators

Because these definitions are probabilistic, they are subject to possible systematic and statistical errors, in particular for small posets. In some cases the systematic errors can be modeled and corrected for, but in general neither type of error is worrisome if they are used only for posets uniformly embedded in Minkowski space. However, these methods are the first steps toward addressing the question of recovering useful information from more general posets, the ones that may arise from sprinklings in curved manifolds or nonmanifoldlike ones. In those settings any noninteger values obtained for the dimensionality may well not be due to the same systematic effects or statistical fluctuations, and it becomes important to identify

an approach to dimensionality that in Minkowski space is accurate even when applied to small regions, since these regions are subject of higher statistical fluctuations, and that can possibly be modeled to maximize its precision.

The main criterion for comparing the various approaches will be based on accuracy (rather than precision, for reasons that we will explain below) using numerical simulations and posets obtained from sprinklings in flat space. Specifically, the Minkowski posets are generated by sprinkling N points at random inside an Alexandrov neighborhood $A(p, q)$ in d-dimensional Minkowski space; p and q themselves will be labeled p_0 and p_{N+1} in the discrete poset; and the latter will therefore be of the form $\mathcal{C} = \{p_i \mid i = 0, ..., N + 1\}$ with $\{p_1, ..., p_N\} = A(p_0, p_{N+1})$.

One advantage of using $\mathbf{L}$ to estimate the dimension is that from its powers one can read off the number of paths of any given length; more precisely, for any $k \geq 1$ the number of paths of length k between any two p_i and p_j is

$$n_k(i, j) = (L^k)_{ij} \ , \tag{4.6}$$

while a similar relation using $\mathbf{R}$ can be used to count chains in the poset.

Figure 4.4 shows the estimated dimension, calculated using (1.10),

$$d = \log_2 N/n$$

for values of N in the range $100 \leq N \leq 1500$ in $d = 2$, 3, 4 and 5 dimensions. For each value of d and N, 15 different Minkowski posets were obtained from random point sprinklings in flat spacetime; the error bars show the standard deviations for the 15 corresponding d estimates. What the figure shows is that, in addition to statistical fluctuations that decrease in size for large N and grow for large d, the use of (1.10) introduces a systematic error that also decreases with N and increases with d. At least part of this error is due to the fact that because of how it is defined, v is in general smaller than the value given by (1.9).

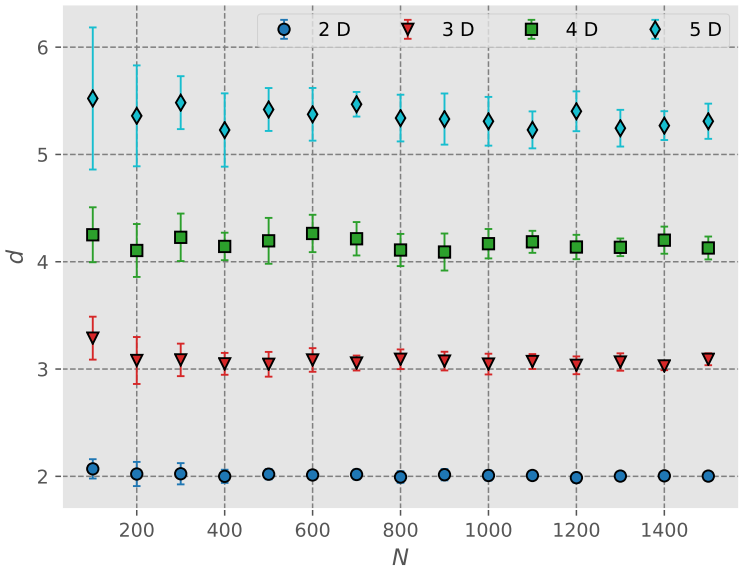

Figure 4.4. The estimated dimension of Minkowski space calculated using the midpoint approach from simulations in $d = 2$, 3, 4 and 5 dimensions as a function of N. The error bars indicate the standard deviation of the results obtained from 15 sprinklings generated for each d and N.

Figure 4.5 shows the estimated dimension, calculated using Eq. (1.13),

$$\frac{\langle C_2 \rangle}{N(N-1)} \approx \frac{1}{4} \frac{\Gamma(d+1)\Gamma(d/2)}{\Gamma(3d/2)}$$

for values of N in the range $100 \leq N \leq 1500$ in $d = 2$, 3, 4 and 5 dimensions. For each value of d and N, 15 different Minkowski posets were obtained from random point sprinklings in flat spacetime; the error bars show the standard deviations for the 15 corresponding d estimates. Because this estimate relies on the exact relation (1.13), rather than on an approximate relationship between discrete and continuum quantities, the figure only shows statistical fluctuations, that again decrease in size for large N and grow with d.

Those results were obtained generating, for each d between 2 and 5 and values of N between 100 and 1500, 15 random Minkowski posets, finding the length $k_{\max}$ of the longest chain in each of them, and averaging the 15 estimated values of $\beta_{d,N}$ obtained from (1.14).

The most accurate estimate for d would be obtained if we had a theoretical value for

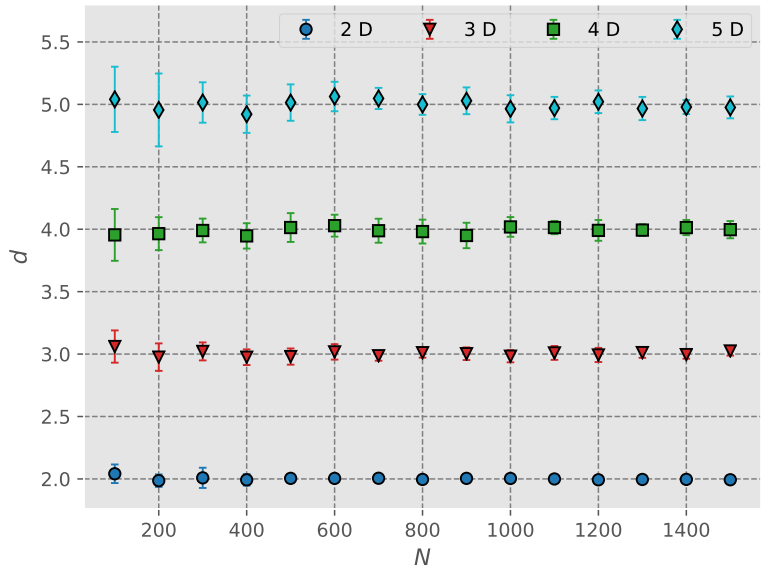

Figure 4.5. The estimated dimension of Minkowski space calculated using the Myrheim-Meyer approach from simulations $d = 2$, 3, 4 and 5 dimensions as a function of N. The error bars indicate the standard deviation of the results obtained from 15 sprinklings generated for each d and N.

$\beta_{d,N}$ available for the given N and for all d in some range, and found a d that solves (1.17) exactly, possibly using numerical methods. In the absence of such an exact expression we could produce approximate values of d centered around the correct ones using for $\beta_{d,N}$ the average of the values obtained from some set of simulations, for example the ones shown in figure 4.7, for each pair of values of (d, N). This would improve the precision of the estimates for d but leave their accuracy essentially unaffected, so we chose not to do it and use $\beta = 2$ in all estimates, which explains the offset of the results shown in figure 4.8, obtained with the same set of values for (d, N).

4.4 Conclusions

Our general goal for this work was to study how to reliably recover the dimensionality of a Minkowski space from the structure of a poset that is embeddable in that space as a random set of points distributed with uniform density. Even in these general terms this question is of interest, but it had already been addressed by various satisfactory approaches

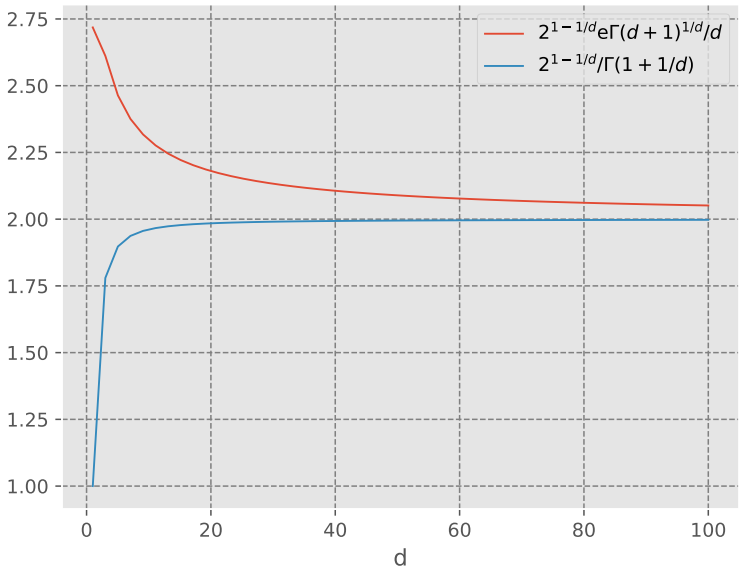

Figure 4.6. Upper and lower bounds on the Brightwell-Gregory parameter β_d as functions of d.

to dimension estimation, including ones based on exact theoretical calculations. In our comparison of the results obtained for numerically simulated, uniformly distributed posets in Minkowski space, however, we were interested in the size of the relative fluctuations in the dimension estimates, in particular for small posets. One reason for this is that we view the study of Minkowski posets as a first step in the study of more general manifoldlike posets, and we expect small enough subsets of posets embeddable in curved Lorentzian geometries to be close enough to Minkowski posets that they can be used to obtain dimensional information.

Since the dimensionalities of manifolds have integer values and all or most of the methods described here (with the possible exception of the Brightwell-Gregory approach) show relatively small fluctuations, if all posets we consider were known to be manifoldlike there would be various approaches we could use. As is well known, however, the vast majority of posets are not manifoldlike (this point is discussed in a little more detail in Ref. [49]), so we would in fact like to be able to extend our method to some of the nonmanifoldlike ones and obtain some information from them, at least when they are close to being manifoldlike in an appropriate sense. In the latter case, an estimate of d might give a value that is close

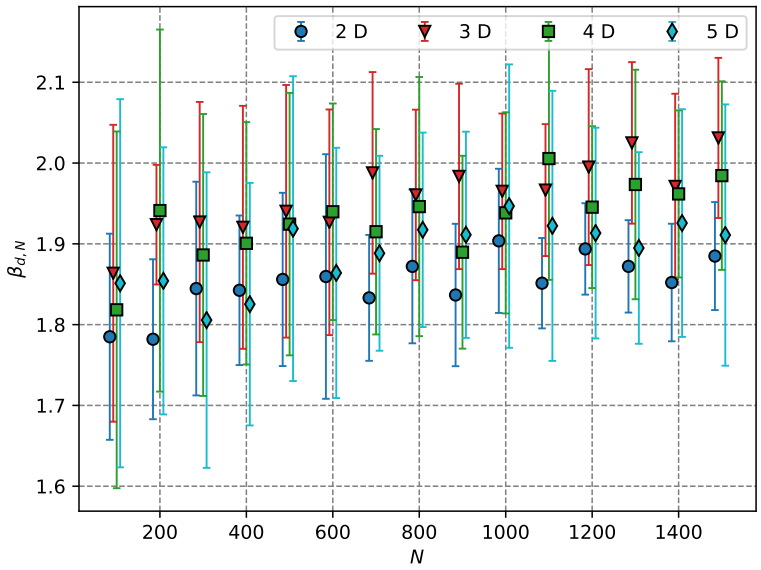

Figure 4.7. The value of $\beta_{d,N}$ for various dimensionalities as a function of N. The error bars indicate the standard deviation of the results obtained from 15 sprinklings generated for each d and N. The simulations are done for causal sets of sizes, 50, 100, ... but we have used small offsets for clearance.

to, but does not coincide with one corresponding to an integer dimension. This is the reason why both small statistical fluctuations and a precise theoretical modeling are important.

Of the approaches we looked at, the best ones in terms of statistical fluctuations are the Myrheim-Meyer one, based on the number of relations C_2, and the one based on the average path length $\bar{k}$. For the latter to be really useful in the sense mentioned above, we would have to be able to calculate exact values for the coefficients $\alpha_{d,N}$. One potential advantage of this method is the fact that α appears to be very weakly dimension-dependent, a fact that might deserve further study. But another reason why we consider our approach promising is that of all the interval-based ones, it is the one that most resembles in spirit the causal spectral dimension approach, based on the probability for paths that start at a common point p to come back together at a point q within a local region in the poset.

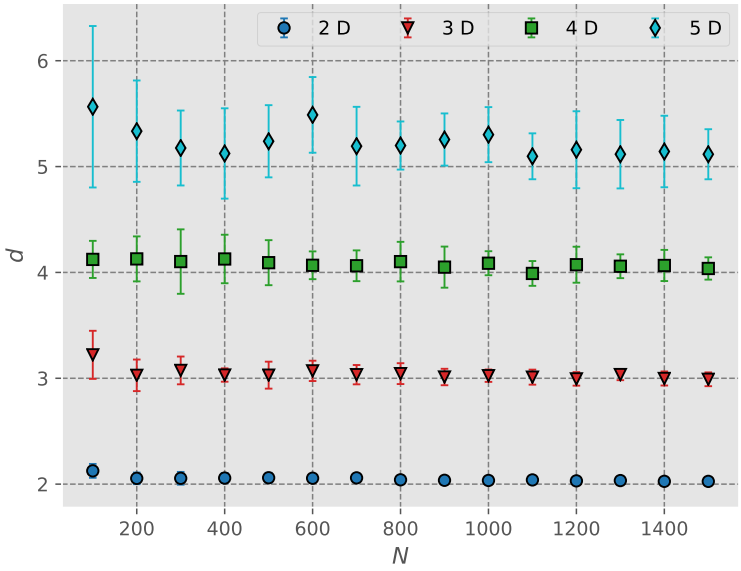

Figure 4.8. The estimated dimension of Minkowski space in the Brightwell-Gregory approach from simulations in $d = 2$, 3, 4 and 5 dimensions as a function of N. The error bars indicate the standard deviation of the results obtained from 15 sprinklings for each value of d and N.

CHAPTER 5

ALEXANDROV NEIGHBORHOODS AND THE SCALAR CURVATURE OF CAUSAL SETS

In this chapter I am proposing a simplified extension of the work done by Glaser and Surya [20], which was originally introduced as a proposal for defining local neighborhoods in causal sets, with some points regarding manifoldlikeness and dimension estimation.The main motivation for this work is to propose an alternative way for finding the discrete equivalent of the scalar curvature without using any support or intermediate scales [29].

5.1 Distribution

One way to obtain a causal set that is embeddable in a spacetime manifold is to sprinkle the points at random through Poisson process on that manifold. As discussed earlier, in such a process the number of points in each volume V in average can be obtained by knowing the density ρ

$$N = \rho V, \tag{5.1}$$

this means that in the discrete case one can measure the volume of a spacetime region by the number of points contained in it. The probability that k points fall in a volume V in the Poisson process is

$$P_k = \frac{(\rho V)^k}{k!} \mathrm{e}^{-\rho V}, \tag{5.2}$$

therefore the mean number of Alexandrov neighborhoods of volume k embedded in an Alexandrov neighborhood within the Minkowski spacetime of dimension d is

$$\langle a_k^0 \rangle = \rho \int_{\mathcal{A}} \mathrm{d}^d x \frac{(\rho V_{x,p})^k}{k!} e^{-\rho V_{x,p}}, \tag{5.3}$$

where the superscript 0 indicates flat spacetime, $\mathcal{A}$ is the bigger Alexandrov neighborhood which is our manifold and $V_{x,p}$ is the volume of the one obtained from the point x and the maximal point p. From now on for simplicity we drop the mean $\langle\rangle$ sign. The mean number of Alexandrov neighborhoods of any arbitrary volume can be obtained from the number of empty ones ($k = 0$) as follows

$$a_k^0 = \rho \frac{(-\rho)^k}{k!} \frac{\partial^k}{\partial \rho^k} \left(\frac{a_0^0}{\rho} \right). \tag{5.4}$$

To simplify the integral, we can use the null coordinates u and v defined by

$$u = (t + r)/\sqrt{2} \; v = (t - r)/\sqrt{2}, \tag{5.5}$$

with $r = (\sum_{i=1}^{d-1} x_i^2)^{1/2}$and expand the exponential to get the following form

$$\begin{aligned} \frac{a_0^0}{\rho} &= \int_{\mathcal{A}} \mathrm{d}^d x \mathrm{e}^{-\rho V_{x,p}} = \int\int\int \mathrm{d}t \; \mathrm{d}r \; \mathrm{d}\Omega \; r^{d-2} \sum_{n=0}^{\infty} \frac{(-\rho V_{x,p})^n}{n!} \\ &= 2^{d-1} d(d-1) k_d \sum_{n=0}^{\infty} \frac{(-\rho k_d)^n}{n!} \times \\ &\times \int_0^{T/\sqrt{2}} \mathrm{d}v \int_v^{T/\sqrt{2}} \mathrm{d}u \left(\frac{u-v}{\sqrt{2}} \right)^{d-2} \left(T - \sqrt{2} v \right)^{\frac{nd}{2}} \left(T - \sqrt{2} u \right)^{\frac{nd}{2}}, \end{aligned} \tag{5.6}$$

where k_d is the volume of an Alexandrov neighborhood of height one in the continuum. Solving the integral we find

$$\frac{a_0^0}{\rho} = d(d-1) V_0 \sum_{n=0}^{\infty} \frac{(-\rho V_0)^n}{n!} \frac{\Gamma(d-1)\Gamma\left(\frac{dn}{2} + 1\right)}{d(n+1)\Gamma\left(\frac{d}{2}(n+2)\right)}, \tag{5.7}$$

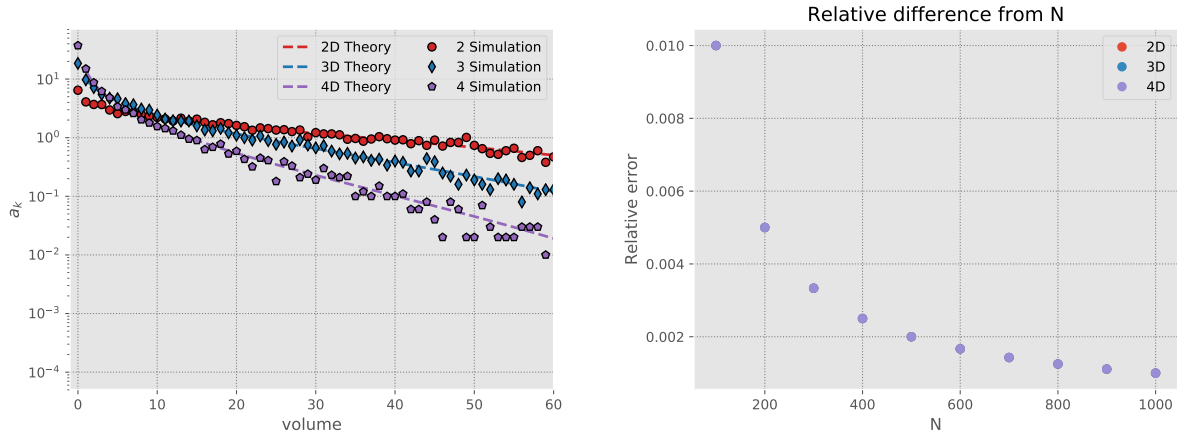

Figure 5.1. Left: The distribution of Alexandrov neighborhoods sharing the same maximal point, with various volumes in a larger Alexandrov neighborhood of volume 100 points and the theoretical estimation. Right: Summing over k should give us the total number of points in the large Alexandrov neighborhood in average. In this figure the relative difference is shown ($|1 - \sum_{k=0}^{n} a_k/N|$).

where V_0 is the volume of the Alexandrov neighborhood $\mathcal{A}$. To find $n_k^{(d)}$ we can take the derivative as suggested in Eq. (5.4)

$$a_k^0 = \frac{\Gamma(d)}{k!}(\rho V_0)^{k+1} \sum_{n=0}^{\infty} \frac{(-\rho V_0)^n}{n!} \frac{\Gamma\left(\frac{d}{2}(n+k)+1\right)}{(n+k+1)\Gamma\left(\frac{d}{2}(n+k+2)\right)}. \tag{5.8}$$

This equation can be written in closed form in terms of generalized hypergeometric functions as is done in Ref. [20], only simpler where they found the distribution of Alexandrov neighborhoods contained in $\mathcal{A}(p,q)$ not necessarily sharing the maximal point,

$$a_k^0 = \frac{\Gamma(d)\Gamma\left(\frac{kd}{2}+1\right)}{\Gamma\left(\frac{d}{2}(k+2)\right)} \frac{(\rho V_0)^{k+1}}{(k+1)!} \, {}_dF_d\left(\left\{k+1, \left[k+\frac{2j}{d}\right]\right\}, \left\{k+2, \left[k+\frac{2j}{d}+1\right]\right\}, -\rho V_0\right), \tag{5.9}$$

where j runs from 1 to $d-1$. In principle the sum over k of these $a_k^{(d)}$ should be very close to the total number of points N in the bigger Alexandrov neighborhood, and we can see that this is true in Fig. (5.1). This equation has the same type of characteristics as what is calculated in Ref. [20] and it is simpler. The shape of the curves is also understandable. If we think of these numbers in analogy with the continuum, in an Alexandrov neighborhood the

constant spacetime distance corresponding to the shorter distances to the maximal point are longer and therefore the probability of finding smaller Alexandrov neighborhoods is larger. In addition, we see from Fig. 5.1 that the theory and simulation agree very well. As expected

$$\sum_k a_k \approx N. \tag{5.10}$$

5.2 Curved Spacetimes

One advantage of finding the distribution of Alexandrov neighborhoods of different volumes all sharing the same maximal point, compared to the distribution calculated in Ref. [20], is that finding the effects of curvature is much easier. Before we start the calculation of the distribution in curved spacetimes it is worthwhile to find the effects of curvature on the volume of an Alexandrov neighborhood, but with the Riemann normal coordinates based at the tip of the Alexandrov neighborhood.

5.2.1 Volume of Curved Alexandrov neighborhoods

The volume of an Alexandrov neighborhood up to the first order in curvature around the mid-point of the neighborhood was previously calculated for 4D by Myrheim in Ref. [9] and for arbitrary dimensions by others in Refs. [58, 41]. However, the mid-point does not necessarily exist in a causal set. In contrast the maximal and minimal points are the ones used to define the Alexandrov neighborhood in the first place and they exist in the causal set. However we want to associate the curvature with elements of the causal set. Therefore, knowing the scalar curvature R at either one of these points is equivalent to knowing it for all points in the causal set. Here I show that using RNC the scalar curvature is the same at both the midpoint and the tip of the light cone, and give the details of the calculation.

As discussed in Ref. [9], the curvature effects can be divided into two parts. The first part comes directly from the volume measure and the second part comes from the boundary

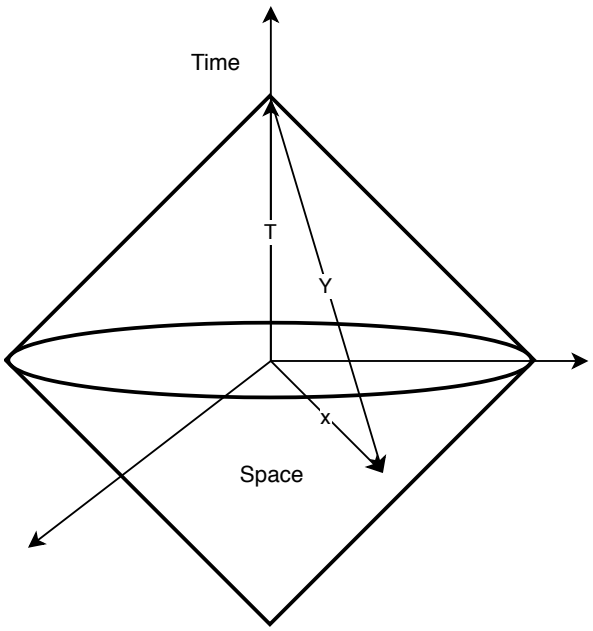

Figure 5.2. Coordinates defined for integration.

of the interval

$$V = \int_{\mathcal{A}} \sqrt{-g}\ \mathrm{d}^d x = \int_{\mathcal{A}_0} \sqrt{1+\delta g}\ \mathrm{d}^d x + \int_{\mathcal{A}-\mathcal{A}_0} \mathrm{d}^d x, \tag{5.11}$$

where $\mathcal{A}$ is the volume of the curved metric Alexandrov neighborhood and $\mathcal{A}0$ is the volume of the spacetime subset which is the Alexandrov neighborhood in the flat metric $\eta_{\mu\nu}$ of the minimal and maximal elements, and we have used the fact RNC are such that $\det(\eta) = 1$. To expand the determinant we need to use the Sylvester's Determinant Theorem which states

$$\det(I_m + AB) = \det(I_n + BA) \tag{5.12}$$

where A is an $m \times n$ and B is an $n \times m$ matrix. The above equation can be derived using

the fact that

$$\begin{pmatrix} I_{m\times m} & O_{m\times n} \\ B_{n\times m} & I_{n\times n} \end{pmatrix} \begin{pmatrix} I_{m\times m} + A_{m\times n}B_{n\times m} & A_{m\times n} \\ O_{n\times m} & I_{n\times n} \end{pmatrix} \begin{pmatrix} I_{m\times m} & O_{m\times n} \\ -B_{n\times m} & I_{n\times n} \end{pmatrix} = \\ = \begin{pmatrix} I_{m\times m} & A_{m\times n} \\ O_{n\times m} & I_{n\times n} + B_{n\times m}A_{m\times n} \end{pmatrix} \tag{5.13}$$

where O is the zero matrix and I is the identity matrix. Taking the determinant of the above formula and the fact that the first and third term are triangular matrices we can simply prove Eq. (5.12). By using Sylvester's theorem we can write

$$\det(X + AB) = \det(X)\det(I + (X^{-1}A)B) = \det(X)\det(I + BX^{-1}A). \tag{5.14}$$

In addition, according to Leibniz formula, the determinant of any matrix is a polynomial from $\mathbb{C}^{n\times n}$ to $\mathbb{C}$, such that it is everywhere differentiable, which means that we can expand the determinant using Jacobi's formula

$$\frac{\mathrm{d}}{\mathrm{d}\alpha}\det(A) = \det(A)\left(A^{-1}\frac{\mathrm{d}A}{\mathrm{d}\alpha}\right). \tag{5.15}$$

For a small variable $\epsilon \ll 1$ we can write

$$\det(I + \epsilon X) = 1 + \mathrm{tr}(X)\epsilon + \mathcal{O}(\epsilon^2). \tag{5.16}$$

It is known that in the RNC, metric takes the form

$$g_{\mu\nu} = \eta_{\mu\nu} - \frac{1}{3}R_{\mu\alpha\nu\beta}X^\alpha X^\beta, \tag{5.17}$$

which by using the result of (5.16), the metric determinant $\det(g)$ up to the first order in

curvature around the maximal point, we have

$$\det(g) = 1 - \frac{1}{6} R_{\mu\nu}(\tau/2, \vec{0}) Y^\mu Y^\nu, \tag{5.18}$$

where $Y^\mu = x^\mu - T^\mu$ and

$$T^\mu = \begin{pmatrix} \tau/2 \\ \vec{0} \end{pmatrix}.$$

Implementing this into the first part of the integral we can find

$$\begin{aligned} \int\limits_{\mathcal{A}_0} \sqrt{1+\delta g}\, \mathrm{d}^d x &= \int\limits_{I_0} \left(1 - \frac{1}{6} R_{\mu\nu}(\tau/2, \vec{0})(x-T)^\mu (x-T)^\nu\right) \mathrm{d}^d x \\ &= V_0 - \frac{1}{6} R_{\mu\nu}(\tau/2, \vec{0}) \int\limits_{\mathcal{A}_0} (x^\mu x^\nu + T^\mu T^\nu - 2 x^\mu T^\nu)\, \mathrm{d}^d x. \end{aligned} \tag{5.19}$$

The third term in parentheses vanishes due to spatial symmetry of the integral domain and therefore the expression reduces to

$$\int\limits_{\mathcal{A}_0} \sqrt{1+\delta g}\, \mathrm{d}^d x = V_0 \underbrace{- \frac{1}{6} R_{\mu\nu}(\tau/2, \vec{0}) \int\limits_{\mathcal{A}_0} (x^\mu x^\nu + T^\mu T^\nu)\, \mathrm{d}^d x}_{A}. \tag{5.20}$$

If we separate the temporal and spatial parts of the part denoted by A we obtain

$$A = -\frac{1}{6} R_{00} (\tau/2)^2 V_0 - \frac{1}{6} R_{00} \int\limits_{\mathcal{A}_0} \mathrm{d}^d x\; t^2 - \frac{1}{6} \sum_{i=1}^{d-1} R_{ii} \int\limits_{\mathcal{A}_0} \mathrm{d}^d x \left(x^i\right)^2, \tag{5.21}$$

where we have once again dropped the odd terms due to symmetry. The result of the last integral term in the above equation is independent of i due to symmetries of the integration. Therefore we can simply change the equation to

$$A = -\frac{1}{6} R_{00} (\tau/2)^2 V_0 - \frac{1}{6} R_{00} \int\limits_{I_0} \mathrm{d}^d x\; \left(t^2 + \frac{r^2}{d-1}\right) - \frac{1}{6} \frac{R}{d-1} \int\limits_{I_0} \mathrm{d}^d x\; r^2, \tag{5.22}$$

where we have used the fact that up to first order in curvature we have

$$-R_{00} + \sum_{i=0}^{d-1} R_{ii} = \eta^{\mu\nu} R_{\mu\nu} = R. \tag{5.23}$$

The above equation has only a simple extra term compared to the results based on RNC expanded around the center of the light cone

$$\int_{\mathcal{A}_0} \sqrt{1+\delta g}\, \mathrm{d}^d x = V_0 \left(1 - \frac{(d+2)}{24(d+1)} R_{00}(\tau/2, \vec{0})\tau^2 - \frac{d}{24(d+1)(d+2)} R(\tau/2, \vec{0})\tau^2\right). \tag{5.24}$$

The boundary contribution is a bit more involved. One should go through finding the null cone surface equations. For that we put the origin on the tip of the cone and look for the equations. Up to first order in curvature the connection becomes

$$\Gamma^{\mu}{}_{\alpha\beta} = \frac{1}{2} g^{\mu\lambda} \left(\partial_\alpha\ g_{\lambda\beta} + \partial_\beta\ g_{\alpha\lambda} - \partial_\lambda\ g_{\alpha\beta}\right) = \frac{1}{3}\left(2R^{\mu}{}_{\beta\epsilon\alpha} + R^{\mu}{}_{\epsilon\alpha\beta}\right) Y^{\epsilon}. \tag{5.25}$$

In the Minkowski spacetime we have

$$\frac{\mathrm{d}^2 x^\mu}{\mathrm{d}\lambda^2} = 0, \tag{5.26}$$

for the geodesic equation which leads to

$$x^\mu = A^\mu \lambda + B^\mu, \tag{5.27}$$

where A^μ and B^μ are constant vectors with respect to the affine parameter. Using eq. (5.25) we can write the geodesic equations for curved spacetimes

$$\frac{\mathrm{d}^2 x^\mu}{\mathrm{d}\lambda^2} - \frac{2}{3} R^{\mu}{}_{\beta\alpha\epsilon} (x - T)^\epsilon \frac{\mathrm{d}x^\alpha}{\mathrm{d}\lambda} \frac{\mathrm{d}x^\beta}{\mathrm{d}\lambda} = 0. \tag{5.28}$$

The second part is already of the first order, so in it we use the Minkowski solution for $x^\mu(\lambda)$,

$$\frac{\mathrm{d}^2 x^\mu}{\mathrm{d}\lambda^2} - \frac{2}{3} R^\mu{}_{\beta\alpha\epsilon}(B-T)^\epsilon A^\alpha A^\beta = 0, \tag{5.29}$$

which gives as first order solution in curvature

$$x^\mu(\lambda) = c^\mu \lambda^2 + A'^\mu \lambda + B'^\mu, \tag{5.30}$$

$$c^\mu \equiv \frac{1}{3} R^\mu{}_{\beta\alpha\epsilon}(B-T)^\epsilon A^\alpha A^\beta. \tag{5.31}$$

The boundary of the lower half of the Alexandrov neighborhood will be given by the same equations, with the difference that

$$c^\mu \equiv \frac{1}{3} R^\mu{}_{\beta\alpha\epsilon}(B+T)^\epsilon A^\alpha A^\beta. \tag{5.32}$$

Now instead of parametric form we need a relationship between time and spatial coordinates. The curved version of the Alexandrov neighborhood can be considered as a map from flat Alexandrov neighborhood in the Minkowski spacetime to the curved spacetime. We set one tip of the Alexandrov neighborhood at $(\tau/2, \vec{0})$ and the other tip at $(-\tau/2, \vec{0})$. Having this in mind we can find the two coinciding null cones. Up to the first order in curvature we have

$$A'^\mu = A^\mu + \tilde{A}^\mu(R).$$

The general null congruence of geodesics can be identified by

$$\begin{aligned} & g_{\mu\nu} A'^\mu A'^\nu = 0 \Rightarrow \left(\eta_{\mu\nu} - \frac{1}{3} R_{\mu\alpha\nu\beta}(x-T)^\alpha (x-T)^\beta\right) A'^\mu A'^\nu = 0 \\ & \Rightarrow \eta_{\mu\nu} A^\mu \tilde{A}^\nu = \frac{1}{6} R_{\mu\alpha\nu\beta} A^\mu A^\nu (B-T)^\alpha (B-T)^\beta. \end{aligned} \tag{5.33}$$

We define the spherical coordinates as follows

$$r^2 \equiv \sum_{i=0}^{d-1} \left(x^i\right)^2 = \lambda^2 + 2A_i\tilde{A}^i(R)\lambda^2 + 2c_iA^i\lambda^3 \tag{5.34}$$

$$t = c^0\lambda^2 + A'^0\lambda + B'^0. \tag{5.35}$$

Due to second order of these equation there will be two answers, but the physical one is the one which in the limit $R = 0$ does not diverge

$$\lambda = -\frac{(B'^0 - t)}{A^0} + \frac{(B^0 - t)}{(A^0)^2}\tilde{A}^0(R) - \frac{(B^0 - t)^2}{(A^0)^3}c^0. \tag{5.36}$$

Substituting this in Eq. (5.34) we get

$$r = \pm\left(\left(c_iA^i + \frac{c^0}{A^0}\right)\frac{(B^0 - t)^2}{(A^0)^2} + \frac{B^0 - t}{A^0}\left(A_i\tilde{A}^i(R) - \frac{\tilde{A}^0(R)}{A^0}\right) + \frac{B^0 - t}{A^0}\right) \tag{5.37}$$

For a null ray moving forward in time we choose $A_\mu = (-1, \vec{A})$ and for a null ray that is moving backward in time we choose $A_\mu = (+1, \vec{A})$. The first term in Eq. (5.37) can be rewritten and calculated as

$$c_iA^i + \frac{c^0}{A^0} = c_iA^i + \frac{c^0A^0}{(A^0)^2} = c_iA^i - c_0A^0 = c_\mu A^\mu$$

$$c_\mu A^\mu = \frac{1}{3}R_{\mu\alpha\beta\epsilon}A^\alpha A^\beta(B - T)^\epsilon A^\mu = 0, \tag{5.38}$$

where in the last part we have used the symmetry properties of the Riemann curvature tensor. For the second term we can use the null condition Eq. (5.33). Up until now all the above can be true for any null geodesic, but to get the Alexandrov neighborhood we need to impose some conditions by defining the tip of the light cone. For a null ray that starts from

the origin and creates the past light cone of the maximal element we have

$$B^{\mu} = \begin{pmatrix} \tau/2 \\ \vec{0} \end{pmatrix}, \tag{5.39}$$

and for consistency we should choose the "$-$" sign in Eq. (5.37),

$$r = -t + \tau/2 \tag{5.40}$$

and we get no curvature correction up to first order, precisely because of Eq. (5.39). For the future light cone of the minimal element in the Alexandrov neighborhood we have

$$B^{\mu} = \begin{pmatrix} -\tau/2 \\ \vec{0} \end{pmatrix}, \tag{5.41}$$

and again to be consistent we need to take the "$-$" sign, so

$$r = \left(\frac{1}{6} R_{i0j0} A^i A^j \tau^2\right)(\tau/2 + t) + (\tau/2 + t). \tag{5.42}$$

The boundary term can be solved by first solving the following integral

$$\begin{aligned} \int_I \mathrm{d}\Omega \int_0^{\tau/2} \mathrm{d}r r^{d-2} \int_{\left(-\frac{1}{6} R_{i0j0} A^i A^j \tau^2 + 1\right) r - \tau/2}^{-r+\tau/2} \mathrm{d}t &= \int \mathrm{d}\Omega \int_0^{\tau/2} \mathrm{d}r r^{d-2} \left(-2r + \tau + \frac{1}{6} R_{i0j0} A^j A^i \tau^2\right) \\ &\approx V_0 \left(1 + \frac{1}{3} R_{00} \left(\frac{\tau}{2}\right)^2\right) \end{aligned} \tag{5.43}$$

where we have expanded in curvature up to first order and used the fact that $A^i = x^i/r = \Omega^i$ and

$$\int \mathrm{d}\Omega \left(A^i\right)^2 = \frac{A_d}{d-1}, \tag{5.44}$$

where A_d is the area of a unit $d-1$ sphere. The contribution only due to the boundary

therefore becomes

$$\delta V_{\text{boundary}} = V_0 \frac{\tau^2}{12} R_{00}. \tag{5.45}$$

Adding the boundary effect and the volume effect we find

$$V_{\text{curved}} = V_{\text{flat}} \left(1 - \frac{d}{24(d+1)} R_{00}(\tau/2, \vec{0})\tau^2 - \frac{d}{24(d+1)(d+2)} R(\tau/2, \vec{0})\tau^2 \right). \tag{5.46}$$

This equation proves that $R(\tau/2, \vec{0}) = R(0, \vec{0})$ and $R_{00}(\tau/2, \vec{0}) = R_{00}(0, \vec{0})$, because the equation has the exact form as it was derived in Refs. [41, 58].

5.3 Distribution in Curved Spacetimes

With the calculations in the previous section we are able to calculate the distribution of Alexandrov neighborhoods volumes in the curved spacetimes up to first order in curvature at the tip. The average number of Alexandrov neighborhoods sharing the same maximal point in a curved spacetime will be similar to the Minkowski space case but now the metric determinant is involved

$$a_k = \rho \int_{\mathcal{A}} \mathrm{d}^d x \, \sqrt{-g} \frac{(\rho V_{x,p})^k}{k!} \mathrm{e}^{-\rho V_{x,p}} = \rho \frac{(-\rho)^k}{k!} \frac{\partial^k}{\partial \rho^k} \left(\frac{n_0^{(d)}}{\rho} \right). \tag{5.47}$$

Expanding a_0 up to first order in curvature gives us the following result

$$a_0 = \int_{\mathcal{A}_R} \mathrm{d}^d x \, \mathrm{e}^{-\rho \, {}_{\mathrm{f}}V_{x,p}} - \rho^2 \int_{\mathcal{A}_0} \mathrm{d}^d x \, \delta V \mathrm{e}^{-\rho \, {}_{\mathrm{f}}V_{x,p}} - \frac{\rho}{6} R_{\mu\nu}(\tau/2, \vec{0}) \int_{\mathcal{A}_0} \mathrm{d}^d x \, x^\mu x^\nu \mathrm{e}^{-\rho \, {}_{\mathrm{f}}V_{x,p}} \tag{5.48}$$

where $fV_{x,y}$ is the volume of Alexandrov neighborhood in a flat spacetime, and ${}_{\mathrm{f}}a_0$ is the distribution of empty Alexandrov neighborhoods in flat spacetime which was already

calculated in the previous section,

$$\begin{aligned}
\delta V &= {}_{\rm f}V_{x,p}\left(\alpha_d R_{00}(\tau/2,\vec{0}) + \beta_d R(\tau/2,\vec{0})\right), \qquad (5.49)\\
\alpha_d &= -\frac{d}{24(d+1)}\tau^2,\\
\beta_d &= -\frac{d}{24(d+1)(d+2)}\tau^2.
\end{aligned}$$

Using Eq. (5.49) in Eq. (5.48) we get

$$\begin{aligned}
\frac{a_0}{\rho} = \sum_{i=1}^{3} I_i = \int\limits_{\mathcal{A}_R} {\rm d}^d x\ {\rm e}^{-\rho\ {\rm f}V_{x,p}} - \frac{1}{6}R_{\mu\nu}\int\limits_{\mathcal{A}_0} {\rm d}^d x\ x^\mu x^\nu\ {\rm e}^{-\rho\ {\rm f}V_{x,p}}\\
-\rho\int\limits_{\mathcal{A}_0} {\rm d}^d x\ \left(\alpha_d R x^\mu x^\nu - \beta_d R\tau_{x,p}^2\right)\ {}_{\rm f}V_{xp}{\rm e}^{-\rho\ {\rm f}V_{xp}}, \qquad (5.50)
\end{aligned}$$

where the first integral contains the zeroth order term. Solving integrals one by one we can write

$$I_1 = V_0\sum_{n=0}^{\infty}\left\{\frac{(-\rho V_0)^n}{n!}\frac{\Gamma(d)\Gamma(1+\frac{dn}{2})}{(n+1)\Gamma(\frac{d}{2}(n+2))} + \frac{d-1}{6}\frac{\Gamma(d+1)\Gamma(1+\frac{dn}{2})}{2\Gamma(1+\frac{d}{2}(n+2))}R_{00}\tau^2\right\}. \qquad (5.51)$$

$$\begin{aligned}
&I_2 =\\
&-R_{00}V_0\sum_{n=0}^{\infty}\frac{(-\rho V_0)^n}{n!}\frac{\Gamma(d+1)(\frac{\tau}{2})^2}{24\Gamma(-\frac{dn}{2})}\left\{-\frac{4\left(\Gamma(\frac{dn}{2})\Gamma(1-\frac{dn}{2})+\Gamma(\frac{d(n+2)}{2})\Gamma(1-\frac{d(n+2)}{2})\right)}{d(n+1)\Gamma(\frac{d}{2}(n+2))} -\right.\\
&\left.-\frac{4d\left(\Gamma(\frac{dn}{2})\Gamma(1-\frac{dn}{2})+\Gamma(\frac{d(n+2)}{2})\Gamma(1-\frac{d(n+2)}{2})\right)}{\Gamma(2+\frac{d}{2}(n+2))} + \frac{(4+n(dn+2))\Gamma(-1-\frac{d}{2}(n+2))}{n+1}\right\} +\\
&-\frac{1}{6}d(d-1)RV_0(\tau/2)^2\sum_{n=0}^{\infty}\frac{(-\rho V_0)^n}{n!}\frac{\Gamma(d+1)\Gamma(\frac{dn}{2})\Gamma(1-\frac{dn}{2})}{(dn+d+2)\Gamma(-\frac{dn}{2})\Gamma(2+\frac{d}{2}(n+2))} \qquad (5.52)
\end{aligned}$$

$$I_3 = \rho V_0^2 (\tau/2)^2 \sum_{n=0}^{\infty} \frac{(-\rho V_0)^n}{n!} \times$$
$$\times \left\{ R \frac{((2+d(n+1))(2+d(n+3))\beta_d + d\alpha_d)\Gamma(d+1)\Gamma(\frac{d(n+1)}{2})\Gamma(1-\frac{d(n+1)}{2})}{(2+d(2+n))\Gamma(-\frac{d(n+1)}{2})\Gamma(2+\frac{d(n+3)}{2})} + \right.$$
$$\left. + \alpha_d R_{00} \frac{(4(n+3)+d(d(n+2)(5+n(n+2)))\,\Gamma(d+1)\Gamma(\frac{d(n+1)}{2})\Gamma(1-\frac{d(n+1)}{2})}{4(n+2)(d(n+2)+2)\Gamma(-\frac{d(n+1)}{2})\Gamma(2+\frac{d(n+3)}{2})} \right\}. \quad (5.53)$$

To find the corrections to $n_k^{(d)}$, we are going to use Eq.(5.4)

$$a_k = \rho(-\rho)^k \frac{\partial^k}{\partial \rho^k} \sum_{i=1}^{3} I_i = \sum_{i=1}^{3} A_i. \quad (5.54)$$

After a very long algebra similar to what is done in Ref. [20] the sums can be evaluated and written in a closed form

$$A_1 = a_k^0 + \frac{d-1}{12} N^{k+1} R_{00} \tau^2 \Gamma(d+1) \frac{\Gamma(\frac{dk}{2}+1)}{\Gamma(\frac{dk}{2}+1+d)} \times$$
$$\times \; {}_dF_d(\{k+\tfrac{2(j+1)}{d}\}; \{k+\tfrac{2(j+1)}{d}+1\}; -N), \quad (5.55)$$

where $j = 0, \cdots, d-1$, and

$$
\begin{aligned}
A_2 = & -\frac{1}{6} R_{00} N^{k+1} \Gamma(d+1)(\tau/2)^2 \times \\
& \times \left\{ \frac{\Gamma(\frac{kd}{2})\Gamma(k)\Gamma(k+2)}{d\Gamma(\frac{kd}{2}+d)\Gamma^2(k+1)} \; {}_{d+2}F_{d+2}\left(\begin{matrix} \{k+1, k+1, k+\frac{2j}{d}\}; \\ \{k, k+2, k+\frac{2j}{d}+1\}; \\ -N \end{matrix} \right) + \right. \\
& + \frac{(-1)^d}{d} \frac{\Gamma(\frac{kd}{2}+1)\Gamma(k+1)}{\Gamma(\frac{kd}{2}+d)\Gamma(k+2)} \; {}_dF_d\left(\begin{matrix} \{k+1, k+\frac{2\ell}{d}\}; \\ \{k+2, k+\frac{2\ell}{d}+1\}; \\ -N \end{matrix} \right) - \\
& - \frac{d\Gamma(\frac{kd}{2}+1)}{\Gamma(\frac{kd}{2}+d+2)} \; {}_{d+1}F_{d+1}\left(\begin{matrix} \{k+\frac{2(j+1)}{2}\}; \\ \{k+\frac{2(j+1)}{d}+1\}; \\ -N \end{matrix} \right) + \\
& + \frac{(-1)^{d-1} d\Gamma(\frac{kd}{2}+1)\Gamma(\frac{d}{2}(k+2))}{\Gamma(\frac{kd}{2}+d)\Gamma(\frac{d}{2}(k+2)+2)} \; {}_{d+1}F_{d+1}\left(\begin{matrix} \{k+\frac{2\ell}{d}, k+\frac{2m}{d}+1\}; \\ \{k+\frac{2\ell}{d}+2, k+\frac{2m}{d}+3\}; \\ -N \end{matrix} \right) + \\
& + \frac{(-1)^{d+1} d\Gamma(\frac{kd}{2}+1)\Gamma^3(k+1)}{4\Gamma(\frac{kd}{2}+d+2)\Gamma^2(k)\Gamma(k+2)} \; {}_{d+4}F_{d+4}\left(\begin{matrix} \{k+1, k+1, k+1, k+\frac{2s}{d}\}; \\ \{k, k, k+2, k+\frac{2s}{d}+1\}; \\ -N \end{matrix} \right) + \\
& \left. + \frac{d\Gamma(\frac{kd}{2}+1)\Gamma(k+3)\Gamma(k+1)}{2\Gamma(\frac{kd}{2}+d+2)\Gamma^2(k+2)} \; {}_{d+3}F_{d+3}\left(\begin{matrix} \{k+1, k+3, k+\frac{2s}{d}\}; \\ \{k+2, k+2, k+\frac{2s}{d}+1\}; \\ -N \end{matrix} \right) \right\} - \\
& - \frac{R}{6}(d-1) N^{k+1} (\tfrac{\tau}{2})^2 \Gamma(d+1) \frac{\Gamma(k+1+\frac{2}{d})\Gamma(\frac{kd}{2}+1)}{\Gamma(k+2+\frac{2}{d})\Gamma(\frac{kd}{2}+d+2)} \times \\
& \times \; {}_{d+3}F_{d+3}\left(\begin{matrix} \{k+1+\frac{2}{d}, k+\frac{2s}{d}\}; \\ \{k+2+\frac{2}{d}, k+1+\frac{2s}{d}\}; \\ -N \end{matrix} \right) . \qquad (5.56)
\end{aligned}
$$

where $\ell = 1, \cdots, d-1$, $j = 0, \cdots, d$, and $s = 1, \cdots, d+1$.

$$
\begin{aligned}
A_3 = N^{k+2}\Gamma(d+1)\frac{\Gamma(\frac{(k+1)d}{2})}{\Gamma(\frac{(k+2)d}{2}+d+2)}\Bigg\{R\Bigg[d\beta_d\frac{\Gamma^2(k+2+\frac{2}{d})\Gamma(k+4+\frac{2}{d})}{\Gamma^2(k+3+\frac{2}{d})\Gamma(k+1+\frac{2}{d})}\times \\
\times\ {}_{d+5}F_{d+5}\begin{pmatrix}\{k+2+\frac{2}{d},k+2+\frac{2}{d},k+4+\frac{2}{d},k+1+\frac{2g}{d}\};\\ \{k+1+\frac{2}{d},k+3+\frac{2}{d},k+3+\frac{2}{d},k+2+\frac{2g}{d}\};\\ -N\end{pmatrix}+ \\
\alpha_d\frac{\Gamma(k+2+\frac{2}{d})}{\Gamma(k+3+\frac{2}{d})}\ {}_{d+3}F_{d+3}\begin{pmatrix}\{k+2+\frac{2}{d},k+1+\frac{2g}{d}\};\\ \{k+3+\frac{2}{d},k+2+\frac{2g}{d}\};\\ -N\end{pmatrix}\Bigg]+ \\
+\alpha_d R_{00}\Bigg[-\frac{\Gamma(k+2)\Gamma(k+4)\Gamma(k+2+\frac{2}{d})}{d\Gamma^2(k+3)\Gamma(k+3+\frac{2}{d})}\times \\
{}_{d+5}F_{d+5}\begin{pmatrix}\{k+2,k+4,k+2+\frac{2}{d},k+1+\frac{2g}{d}\};\\ \{k+3,k+3,k+3+\frac{2}{d},k+2+\frac{2g}{d}\};\\ -N\end{pmatrix}+ \\
+\frac{g\Gamma(k+\frac{7}{2})\Gamma(k+2+\frac{2}{d})}{2\Gamma(k+\frac{5}{2})\Gamma(k+3+\frac{2}{d})}\ {}_{d+4}F_{d+4}\begin{pmatrix}\{k+\frac{7}{2},k+2+\frac{2}{d},k+1+\frac{2g}{d}\};\\ \{k+\frac{5}{2},k+3+\frac{2}{d},k+2+\frac{2g}{d}\};\\ -N\end{pmatrix}+ \\
+\frac{d\Gamma^{(}k+1)\Gamma(k+2+\frac{2}{d})}{4\Gamma^{(}k)\Gamma(k+3+\frac{2}{d})}\ {}_{d+5}F_{d+5}\begin{pmatrix}\{k+1,k+1,k+2+\frac{2}{d},k+1+\frac{2g}{d}\};\\ \{k,k,k+3+\frac{2}{d},k+2+\frac{2g}{d}\};\\ -N\end{pmatrix}\Bigg]\Bigg\} \qquad (5.57)
\end{aligned}
$$

where we have $g = 1, \cdots, d+2$ and it is integer.

This given the volume distribution of Alexandrov neighborhoods all sharing the same maximal point, up to the first order in curvature. It contains both R_{00} and the Ricci scalar curvature R, therefore it can be either used for identification of the distribution if the spacetime is previously known or it can be solved for R to find the action and this action is defined on the existing points of the causal set because the expansion of volume is about

the tip of the Alexandrov neighborhood which is a point in Alexandrov neighborhood. For 2 dimensions however, since there is only one independent component in the Ricci tensor, this is equivalent to knowledge of the gravitational action.

This proposal has the same property as what was proposed by Benincasa and Dowker, in the sense that it has the same limitation in terms of choosing a frame, but the advantage for this result is that it has emerged from the discrete properties of the spacetime rather than a guess. In a way it is also the discretized version of the scalar curvature in Ref. [30]. The total number of Alexandrov neighborhoods should converge to the total number of points in the original Alexandrov neighborhood regardless of curvature, which provides extra information on the curvature of spacetime.

Since the coefficients of R and R_{00} are k-dependent ($\delta a_k = A_k R + B_k R_{00}$) one can use two values to estimate the scalar curvature

$$R = \frac{B_1 \delta a_0 - B_0 \delta a_1}{A_0 B_1 - A_1 B_0}, \tag{5.58}$$

where ${}_f n_k$ can be estimated using the theoretical value if the dimension is known from an independent method. One can also average a few of the values calculated this way using Alexandrov neighborhoods of different volumes.

Another point that one might be able to deduce from this is the following

$$\sum_k a_k \approx N = N_0 + \tau^2 R \sum_k A_k + \tau^2 R_{00} \sum_k B_k, \tag{5.59}$$

which is precisely the discrete version of the effect of curvature on the volume of an Alexandrov neighborhood, leading to

$$\sum_k A_k = -\rho \frac{d}{24(d+1)(d+2)} \tag{5.60}$$

$$\sum_k B_k = -\rho \frac{(3d+2)}{24(d+1)}. \tag{5.61}$$

CHAPTER 6

CONCLUSIONS

Overall the strongest results are obtained regarding the dimension with the simulations supporting it, however for the length distribution and the Alexandrov neighborhood volume distribution, even though the theoretical ground work is done completely, some simulations are needed to be done to support the theoretical calculations.

The scalar curvature that is calculated here does not depend on a choice of scalar field of compact support, and choice of layers plays no role in the calculation. The work done in Ref. [29] even though is very nice in nature but the freedom in choosing the number of layers and the fact that different number of minimum layers are required for different dimensions makes it a weaker. The solution presented here is purely from discrete calculations and for an embeddable manifoldlike causal set, should work well.

I would like to also propose a method to construct an action which is inspired by study of Machine Learning algorithms, specifically the ones that are used for anomaly detection. This proposal could potentially lead to the identification of manifoldlike causal sets, based on the ideas that were introduced in Chapter 3.

The peak position k_0, and width Δ of the path length distribution, and the total number of paths, create a parameter space in which the manifoldlike causal sets only occupy a tiny region. As a proposal I suggest to use a 3-dimensional normalized Gaussian distribution that is peaked at the average values that correspond to manifoldlike causal sets and decreases exponentially as we move away from those regions. Therefore the weight at which each of

the causal sets would be taken into account is

$$W = \frac{1}{\sqrt{(2\pi)^3 |\mathbf{\Sigma}|}} \exp\left(-\tfrac{1}{2}(x-\mu)^{\mathrm{T}} \mathbf{\Sigma}^{-1} (x-\mu)\right) \tag{6.1}$$

where $\mathbf{\Sigma} = \left\langle (x-\mu)(x-\mu)^{\mathrm{T}} \right\rangle$ in this case is a 3×3 Covariance matrix, $|\mathbf{\Sigma}| = \det(\mathbf{\Sigma})$, and μ is the mean vector. This proposal not only gives higher weight to the manifoldlike causal sets but as an action its derivative is also zero at those regions which is what one generally requires. It is also obvious that cases such as the diamond lattice and KR poset are far away from the peak of this distribution and therefore will have a very small contribution which is very desirable in "path integral" formulation of CST.

BIBLIOGRAPHY

[1] H.W. Hamber, "Quantum Gravity on Lattice," *Gen. Relativ. Gravit.* **41**, 817 (2009)

[2] C. Brans, R. H. Dicke, "Mach's Principle and a Relativistic Theory of Gravitation," *Phys. Rev.* **124**, 925 (1961)

[3] N. Rosen, "A bi-metric theory of gravitation," *Gen. Relativ. Gravit.* **4**, 435 (1973)

[4] E. Berti et *al.* "Testing General Relativity with Present and Future Astrophysical Observations," *Class. Quantum Grav.* **32**, 243001 (2015)

[5] J. Aastrup, J. Grimstrup, "Intersecting Quantum gravity with Noncommutative Geometry - a Review," *SIGMA* **8**, 18 (2012)

[6] Weinberg, Steven. "Ultraviolet divergences in quantum theories of gravitation". In S. W. Hawking; W. Israel. General Relativity: An Einstein centenary survey. Cambridge University Press. pp. 790–831 (1979).

[7] A. Ashtekar, "New variables for classical and quantum gravity," *Phys. Rev. Lett.* **57**, 2244 (1986).

[8] L. Bombelli, J. Lee, D.A. Meyer and R.D. Sorkin, "Spacetime as a causal set," *Phys. Rev. Lett.* **59**, 521 (1987).

[9] J. Myrheim, "Statistical geometry," 1978 preprint, Ref. TH 2538-CERN, unpublished.

[10] G. 't Hooft, "Quantum gravity: a fundamental problem and some radical ideas,", pp. 323-45, in "Recent Developments in Gravitation" (Proceedings of the 1978 Cargese Summer Institute) edited by M. Levy and S. Deser (Plenum, 1979)

[11] S.W. Hawking, King and McCarthy, "A new topology for curved spacetime which incorporates the causal, differential and conformal structures," *J. Math. Phys.* **17** 174 (1976)

[12] D. Malament, "The class of continuous timelike curves determines the topology of spacetime," *J. Math. Phys.* **18** 1399 (1977)

[13] L. Bombelli and D. Meyer, "The origin of Lorentzian geometry," *Phys. Lett.* A **141** (1989) 226-228.

[14] L. Bombelli, J. Tafoya and J. Noldus, unpublished.

[15] L. Bombelli, "Statistical Lorentzian geometry and the closeness of Lorentzian manifolds," *J. Math. Phys.* **41** 6944 (2000).

[16] D. Kleitman and B. Rothschild, "Asymptotic enumeration of partial orders on a finite set," *Trans. Amer. Math. Society* **205**, 205-220 (1975).

[17] "Classical Sequential Growth,"

[18] L. Bombelli, J. Henson and R.D. Sorkin, "Discreteness without symmetry breaking: A theorem," *Mod. Phys. Lett.* A **24** (2009) 2579-2587, and arXiv:gr-qc/0605006.

[19] D. Rideout, P. Wallden, "Emergence of spatial structure from causal sets," *Class. Quantum Grav.* **174**, 12017 (2009)

[20] L. Glaser and S. Surya, "Towards a definition of locality in a manifoldlike causal set," *Phys. Rev.* **D** 88, 124026 (2013), and arxiv:1309.3403.

[21] D. Kelly and W.T. Trotter, "Dimension theory for ordered sets," in *Ordered Sets*, ed. I. Rival, Reidel 1982.

[22] L. Bombelli, *Space-Time as a Causal Set*, PhD dissertation, Syracuse University 1987.

[23] D.A. Meyer, *The Dimension of Causal Sets*, PhD Dissertation, MIT 1988.

[24] G. Brightwell and R. Gregory, "Structure of random discrete spacetime," *Phys. Rev. Lett.* **66** (1991) 260-263.

[25] D.D. Reid, "Manifold dimension of a causal set: Tests in conformally flat spacetimes," *Phys. Rev.* D **6**7 (2003) 024034, arXiv:gr-qc/0207103.

[26] A. Eichhorn and S. Mizera, "Spectral dimension in causal set quantum gravity," arXiv:1311.2530.

[27] A. Eichhorn, S. Mizera and S. Surya, "Echoes of asymptotic silence in causal set quantum gravity," arXiv:1703.08454.

[28] S. Carlip, "Dimension and dimensional reduction in quantum gravity," arXiv:1705.05417; J. Abajian and S. Carlip, "Dimensional reduction in manifold-like causal sets," arXiv:1710.00938.

[29] D. Benincasa and F. Dowker, "The scalar curvature of a causal set," *Phys. Rev. Lett.* **1**04: 181301 (2010), and arXiv:1001.2725.

[30] R. Sverdlov and L. Bombelli, "Gravity and matter in causal set theory," *Class. Quantum Grav.* **26**, 075011 (2009).

[31] R. Sverdlov and L. Bombelli, "Dynamics for causal sets with matter fields: a Lagrangian-based approach," *J. Phys. Conf. Ser.* **174**, 012019 (2009).

[32] M. Buck, F. Dowker, I. Jubb, and S. Surya, "Boundary terms of causal sets," *Class. Quantum. Grav.* **32**, 205004 (2015)

[33] G. Gibbons and S. Hawking, "Action Integrals and Partition Functions in Quantum Gravity," *Phys.Rev.* **D15** 2752 (1977)

[34] J. York, "Role of conformal three-geometry in the dynamics of gravitation," *Phys. Rev. Lett.* **28** 1082 (1972)

[35] S. Johnston, "Feynman Propagator for a Free Scalar Field on a Causal Set," *Phys. Rev. Lett.* **103**, 180401 (2009)

[36] S. Johnston, "Particle propagators on discrete spacetime," *Class. Quantum Grav.* **25** 202001 (2008)

[37] R. Sorkin, "Is the cosmological "constant" a nonlocal quantum residue of discreteness of the causal set type?" *AIPConf. Proc.* **957**, 142 (2007)

[38] F. Dowker, J. Henson, R. Sorkin, "Quantum Gravity Phenomenology, Lorentz Invariance and Discreteness," *Mod. Phys. Lett.* **A19**, 1829 (2004)

[39] M. Aghili, L. Bombelli, B.B. Pilgrim, in preparation.

[40] G. Gibbons, S. Solodukhin, "The Geometry of Small Causal Diamonds," *Phys. Lett.* B **649**, 317 (2007)

[41] M. Roy, D. Sinha, and S. Surya, "Discrete geometry of a small causal diamond," *Phys. Rev.* D**87**, 044046 (2013)

[42] J. Henson, "Constructing an interval of Minkowski space from a causal set," *Class. Quantum Grav.* **23** 29-35 (2006).

[43] S. Major, D. Rideout and S. Surya, "Stable homology as an indicator of manifoldlikeness in causal set theory," *Class. Quantum Grav.* **26**: 175008 (2009).

[44] A. Eichhorn and S. Mizera, "Spectral dimension in causal set quantum gravity," *Class. Quantum Grav.* **31**: 125007 (2014), and arXiv:1311.2530.

[45] Y. Yazdi and M. Kempf, "Towards spectral geometry for causal sets," *Class. Quantum Grav.* **34**: 094001 (2017).

[46] G. Brightwell and R. Gregory, "Structure of random discrete spacetime," *Phys. Rev. Lett.* **66**, 260 (1991).

[47] S. Surya, "Causal set topology," *Theor. Comput. Sci.* **4**05: 188-197 (2008), and arXiv:0712.1648.

[48] N. X, F. Dowker and S. Surya, "Scalar field Green functions on causal sets," *Class. Quantum Grav.* **34**, 124002 (2017)

[49] M. Aghili, L. Bombelli, B. B. Pilgrim, "Path Length Distribution in Two-Dimensional Causal Sets,"

[50] F. Aurenhammer, R. Klein and D.-T. Lee, *Voronoi Diagrams and Delaunay Triangulations*, World Scientific 2013.

[51] L. Santaló, *Integral Geometry and Geometric Probability*, 2nd edition, Cambridge University Press 2004.

[52] R.E. Miles, "Random points, sets and tessellations on the surface of a sphere," *Sankhya: The Indian J. of Stat.* **33** (1971) 145-174.

[53] J.J. García Escudero, "Random tilings of spherical 3-manifolds," *J. Geom. Phys.* **58** (2008) 1451-1464 (doi.org/10.1016/j.geomphys.2008.05.015).

[54] L. Bombelli, "Statistical geometry of random weave states," in V.G. Gurzadyan et al., eds *Proceedings of the Ninth Marcel Grossmann Meeting on General Relativity*, World Scientific 2002.

[55] L. Bombelli, A. Corichi and O. Winkler, "Semiclassical quantum gravity: Statistics of combinatorial Riemannian geometries," *Ann. der Physik* **14** (2005) 499D519, and arXiv:gr-qc/0409006.

[56] S. Surya, "Directions in causal set quantum gravity," arXiv:1103.6272.

[57] F. Dowker, "Introduction to causal sets and their phenomenology," *Gen. Rel. Grav.* **45** (2013) 1651-1667.

[58] G.W. Gibbons and S.N. Solodukhin, "The geometry of small causal diamonds," *Phys. Lett.* **B649** (2007) 317-324, arXiv:hep-th/0703098.

[59] L. Bombelli, "Statistical Lorentzian geometry and the closeness of Lorentzian manifolds," *J. Math. Phys.* **41** (2000) 6944-6958, arXiv:gr-qc/0009018.

[60] M. Aghili, "Simulations of Path Length Distribution and the Dimension," DOI: 10.5281/zenodo.2633359

VITA

Mir Emad Aghili

maghili@olemiss.edu

Education and Certificates

- **PhD**, Quantum Gravity, Causal Sets Theory

  University of Mississippi, Oxford, MS 2015-present

  DISSERTATION - **Manifoldlike Causal Sets**,

- **MS**, General Relativity and Gravitation

  University of Mississippi, Oxford, MS 2012-2015

  THESIS - **Effect of Accelerated Global Expansion on Bending of Light**,

- **MS**, Elementary Particle and High Energy Physics

  Shiraz University, Shiraz, Iran 2010-2012

  THESIS - **Calculation of Deuteron's Magnetic Moment with Use of Simple Quark Model**,

- **BS**, Atomic Physics

  Shiraz University, Shiraz, Iran 2005-2010

  PROJECT - **Stochastic Resonance in Double-Sine Gordon potential well**,

- **Certificate**, Machine Learning

  Online Course, Stanford University Feb 2018

Publications

- **M. Aghili**, L. Bombelli, B. B. Pilgrim, "Discrete Spacetime: a Web of Chains," arXiv:1807.08701 (submitted to *Class. Quantum Grav.*). 2019
- **M. Aghili**, L.Bombelli, B. B. Pilgrim, "Path Length Distribution in Two-Dimensional Causal Sets," *Eur. Phys. J.* **C**, **78** (9), 744. 2018
- **M. Aghili**, B. Bolen, L. Bombelli, "Effect of accelerated global expansion on the bending of light," *Gen. Relativ. Gravit.*, **49** (1) 10. 2017
- E. Berti, et al. "Testing general relativity with present and future astrophysical observations," *Class. Quantum Grav.*, **32** (24), 243001. 2015
- N. Ghahramany, Yazdankish, **M. Aghili**, "Calculation of Deuteron Magnetic Dipole Moment Using Constituent Quarks for All Possible Δ^{++}, Δ^{+}, Δ^{0}, Δ^{-}, p and n Baryon Formations," *Univ. J. Phys. App.*, **7** (3) 236 2013
- **M. Aghili**, L. Bombelli, B. B. Pilgrim, "Gravitational Action as a function of Alexandrov Sets Distribution," (In preparation for submission to *Phys. Rev.* **D**).

Accepted Conference Presentations

- "A measure for manifoldliekness of causal sets," Quantum Gravity on Computer, Stockholm, **Sweden**. 2018
- "A measure for manifoldlikeness of causal sets," APS March Meeting, Columbus, **Ohio**. 2018
- "Using most probable path for finding the dimension of causal sets," Midwest General Relativity Meeting, Ann Arbor, **Michigan**. 2017
- "Effect of global expansion on bending of light", Midwest General Relativity Meeting, Oakland, **Michigan**. 2014

- "Effect of global expansion on bending of light", Mississippi Academy of Sciences, Hattiesburg, **Mississippi**. 2013

Refereeing Journals

- *EPJ* **C**
- *CQG*
- *JMP*

Research Interests

- Causal Set Theory
- Spin-Foam
- Astrophysics
- Complex Systems
- Loop Quantum Gravity
- Gravitational Waves

Computer Skills

- **Programming**: PYTHON, MATLAB, MATHEMATICA, HTML, Shell Scripting, C.
- **Data analysis**: Data cleaning, mining, and analysis, Data Structures
- **Machine Learning**: Linear & Logistic Regression, Neural Networks, SVM, Clustering, Random Forest.
- **Numerical skills**: Numerical Data Analysis, Numerical Simulation, Runge-Kutta, Monte-Carlo.

Memberships

- American Physical Association (APS), Student Affiliate 2013-present
- Member of ΣΠΣ physics honor student society 2015-present
- Society of Physics Students of United States (SPS) 2015-present

- President, Physics Graduate Student Association (PGSA), University of Mississippi 2017-2018
- Vice President, Physics Graduate Student Association (PGSA), University of Mississippi 2016-2017
- Journal Club Coordinator and Editor of "Mississippi Physicist", University of Mississippi 2016-2017

Honors

- Department Fellowship — Summer 2018
- DGRAV travel grant — 2018
- Graduate School Dissertation Fellowship — 2018
- Perimeter Institute for Theoretical Physics travel grant — 2017
- Research Assistant, University of Mississippi — Summers 2013, 16, 17

Teaching Experience

- **Instructor**- Phys 107
  University of Mississippi — Fall 2017
- **LAB Instructor**- Astronomy
  University of Mississippi — 2012-2017
- **LAB Instructor**- Engineering Physics
  Shiraz University — 2010-2012
- **Teaching Assistant**- E & M., Q. Mech. and Math. Phys.
  Shiraz University — 2005-2012

References

Luca Bombelli, PhD.

Professor

Lewis Hall 108A

Department of Physics and Astronomy

The University of Mississippi

Department Chair

phone: (662) 915-5319

e-mail: luca@phy.olemiss.edu

Richard Raspet, PhD.

Professor Emeritus

NCPA 2018

Department of Physics and Astronomy

National Center for Physical Acoustics

The University of Mississippi

phone: (662) 915-5888

e-mail:raspet@olemiss.edu

Alakabha Datta, PhD.

Associate Professor

Lewis Hall 209

Department of Physics and Astronomy

The University of Mississippi

phone: (662) 915-5611

e-mail:datta@phy.olemiss.edu

Tibor Torma, PhD.

Assistant Professor

Lewis Hall 208

Department of Physics and Astronomy

The University of Mississippi

phone: (662) 915-5627

e-mail: ttorma@phy.olemiss.edu